Final Report

Experimental Investigations of Two-Phase Cooling in Microgap Channel

AOARD Reference Number: AOARD-10-4073

AOARD Program Manager: Dr. Rengasamy Ponnappan

Period of Performance: 01/04/2010 – 31/03/2011

Submission Date: April 25, 2011

Principal Investigator:

Dr. Poh Seng Lee

Assistant Professor of Mechanical Engineering

National University of Singapore

Report Documentation Page

Form Approved
OMB No. 0704-0188

1. REPORT DATE	2. REPORT TYPE	3. DATES COVERED
16 MAY 2011	**Final**	**22-04-2010 to 21-04-2011**

4. TITLE AND SUBTITLE
Investigations of Two-Phase Microgap Channel Cooling

5a. CONTRACT NUMBER
FA23861014073

5b. GRANT NUMBER

5c. PROGRAM ELEMENT NUMBER

6. AUTHOR(S)
Po-Seng Lee

5d. PROJECT NUMBER

5e. TASK NUMBER

5f. WORK UNIT NUMBER

7. PERFORMING ORGANIZATION NAME(S) AND ADDRESS(ES)
National University of Singapore,9 Engineering Drive 1,117576,Singapore,NA,NA

8. PERFORMING ORGANIZATION REPORT NUMBER
N/A

9. SPONSORING/MONITORING AGENCY NAME(S) AND ADDRESS(ES)
AOARD, UNIT 45002, APO, AP, 96338-5002

10. SPONSOR/MONITOR'S ACRONYM(S)
AOARD

11. SPONSOR/MONITOR'S REPORT NUMBER(S)
AOARD-104073

12. DISTRIBUTION/AVAILABILITY STATEMENT
Approved for public release; distribution unlimited

13. SUPPLEMENTARY NOTES

14. ABSTRACT
In this study, experiments have been performed in order to examine two-phase flow boiling in a silicon microgap based heat sink having gap height of 190μm, 285μm and 380μm, using water with inlet temperature of 86˚C. The effects of mass flux and heat flux on heat transfer coefficient and pressure drop characteristics were examined by varying mass flux ranging from 420 Kg/m?s to 970 Kg/m?s and effective heat flux up to 100 W/cm?. An array of integrated micro-temperature sensors allows local heat transfer coefficients to be determined. The fluid temperatures and pressure drop across the microgap array were also measured. The size effects on different parameters have been investigated. The extensive microgap boiling experiments and analysis has led to some important findings listed in this final report.

15. SUBJECT TERMS
Heat Transfer, Miccrogap channel, Miccrogap channel, Electronics cooling, Electronics cooling

16. SECURITY CLASSIFICATION OF:			17. LIMITATION OF ABSTRACT	18. NUMBER OF PAGES	19a. NAME OF RESPONSIBLE PERSON
a. REPORT	b. ABSTRACT	c. THIS PAGE			
unclassified	**unclassified**	**unclassified**	**Same as Report (SAR)**	**67**	

Table of Contents

Acknowledgements

The Author gratefully acknowledges the Asian Office of Aerospace Research & Development (AOARD) for their financial support with reference no. ..... for this work.

Abstract

Microsystems are widely used in high heat flux situations due to their low cost and high potential applications in many fields such as space, communication, biology and industry. Flow boiling is very important in such devices for cooling applications. Utilizing the latent heat of coolant, flow boiling can dissipate significantly higher heat fluxes while requiring smaller rates of coolant flow than its single phase counterpart. Another advantage of convective boiling process is the greater temperature uniformity across the heat sinks as the phase change takes place at the fluid saturation temperature. In spite of these appealing attributes, the complex nature of convective boiling and two phase flow and the associated flow instabilities and flow reversal issues are still not well understood and these have impeded their wide implementation in practical applications. To address some of these issues, the concept of the two-phase microgap channel coolers is recently proposed to directly cool the heat sources. The two-phase microgap channel coolers can potentially mitigate the flow instabilities and flow reversal issues inherent with two-phase microchannel heat sinks as the vapour generated has room to expand both spanwise and downstream instead of being forced upstream. As the concept of the two-phase microgap channel cooler is still very new, more work should be done to advance the fundamental understanding of the two-phase flow and heat transfer associated with it and the underlying mechanism(s).

1. Introduction

1.1 Background

In recent years, electronic devices, such as micro-processors and lasers, have increased in power consumption and reduced in physical size. This has led to an increasing intensity in heat generation that needs to be removed during normal operation. In particular, Thermal and power management are widely considered to be the crucial links in the ability to embrace high-performance computing technology in military systems designs [1-2]. Heat dissipation from defence applications is projected to exceed 1000W/cm^2 in the near future as shown in Figure 1. This is primarily due to the greater functionalities and higher packaging densities. To ensure safe and reliable operations, there is a need for high capacity thermal management techniques. It therefore seems likely that new methods will be needed in the not too distant future. One possibility is to use a boiling fluid as the coolant, as this would transfer significantly more heat than its single-phase equivalent. This has led to an abundance of research into flow boiling in microchannels. Utilizing the latent heat of coolant, flow boiling can dissipate significantly higher heat fluxes while requiring smaller rates of coolant flow than its single phase counterpart. Another advantage of convective boiling process is the greater temperature uniformity across the microchannel heat sinks as the phase change take place at the fluid saturation temperature. In spite of this appealing attributes, the complex nature of convective boiling and two phase flow in microchannels is still not well understood and this has impeded their wide implementation in practical applications. The major issues that require urgent attention include flow instabilities and flow reversal; lack of good fundamental understanding of the underlying mechanism for two phase flow and heat transfer in microscale domain and the associate lack of generally accepted models for predicting two phase pressure drop and boiling heat transfer in micro/ mini channels. To address some of these issues, the concept of the two-phase microgap channel coolers is recently proposed to directly cool the heat sources. Microgap coolers provide direct contact between chemically inert, dielectric fluids and the back surface of an active electronic component, thus eliminating the significant interface thermal resistance associated with Thermal Interface Materials and/or solid-solid contact between the component and a microchannel cold plate. In addition, the two-phase microgap channel coolers can potentially mitigate the flow instabilities and flow reversal issues inherent with two-phase microchannel heat sinks as the vapour generated has room to expand both spanwise and downstream instead of being forced

upstream. Moreover, it can be used for mitigating hotspots as it maintains a uniform fluid layer over the heated surface.

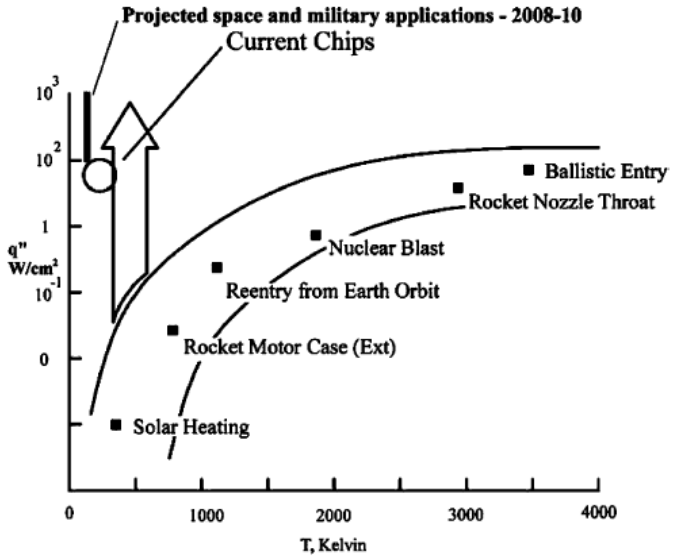

Figure 1: Projected cooling demands in comparison to other man-made thermal systems [3].

1.2 Application

A defence application that calls for high capacity cooling is the High Energy Laser (HEL) system. For practical deployment on tactical platforms, the laser and cooling system must be compact, lightweight and reliable. The inherent inefficiencies of the laser components, large power requirements and high heat fluxes (500 W/cm^2) impose the primary obstacle facing HEL system deployment. Single-phase cooling approaches fail to address these challenges due to the extremely large coolant flow rates required for tight temperature control (±2°C) in laser devices. This traditional approach results in large, heavy cooling systems that are not viable options for tactical platforms, such as a fighter jet, tank, or gunship. Two-phase microgap channel coolers, on the other hand, can result in smaller pumps, less power consumption, reduced fluid inventory and more efficient heat transfer enabling tactical deployment of these systems.

Active radar systems require advanced thermal management technology to provide higher heat dissipation and allow the power amplifiers and other electronic components to operate at higher power densities, high temperatures and high frequencies which substantially enhance the system's efficiency and reduce the size and weight of power amplifiers and the associated

T/R modules, offering the advantages such as light weight, small size, longer service life, and improved capability and reliability. The increased power densities, however, will inevitably generate more waste heat, requiring more advanced thermal management. The next-generation active radar systems (e.g. X-band radars) based on GaN-based technology can create high heat fluxes up to 500-1,000 W/cm^2. Therefore, more advanced thermal management technology, like that of two-phase microgap channel coolers need to be developed, to provide the required ultra high-efficiency heat dissipation. Other defence applications that could utilize two-phase microgap channel coolers include the next generation of high power Integrated Power Systems (IPSs), electromagnetic weapons (EWs) and aviation electronics.

1.3 Objectives

The objectives of the project are:

1. To obtain a better fundamental understanding of the two-phase flow and heat transfer processes in micro-gap channel over a range of gap dimension.
2. To assess the ability of the two-phase microgap coolers in mitigating flow instabilities and flow reversal.
3. To use the two-phase micro-gap channel cooling technology for hotspots mitigation.

1.4 Scope

The scope of the project includes:

1. To conduct careful and systematic experimental investigations to obtain accurate flow boiling heat transfer and pressure drop data over a range of vapor qualities, heat fluxes, mass fluxes, and channel dimensions.
2. To explore the effectiveness of microgap channel for mitigate flow instabilities and flow reversal.
3. To evaluate the characteristics of two phase flow boiling in microgap channel.
4. To explore the application of two-phase micro-gap channel cooling technology for hotspots mitigation.

2. Literature Review

Dielectric liquid flowing through heated microchannel or microgap channel undergoes phase change. This vapor/liquid mixtures flowing in miniature channels aggregate into four primary two-phase flow regimes: bubbly, intermittent, annular and Dryout [4-6].

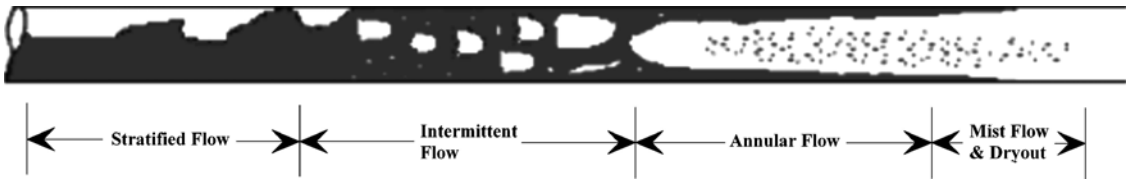

Figure 2: Diagram of a developing flow in a horizontal channel [40].

Development of bubbly flow is noted by a small volumetric fraction of bubbles within the liquid flow. In intermittent flow, these bubbles coalesce and form “slugs” in the flowing liquid. Annular flow, which is associated with thin liquid layers flowing along the outer walls of the channel and the vapour flows in the center of the channel called vapor core. This is thermally advantageous, due to the high heat transfer rates associated with the evaporation of thin liquid layers. Thin liquid layers have low resistance to thermal diffusion and evaporation of liquid into the vapor core can promote the removal of substantial thermal energy from the walls. As the layer thins, the heat transfer rate increases. However, local dryout can occur with extremely thin films and then propagate to complete dryout. In horizontal channel, at low two phase flow rate, a stratified pattern may also occur in which the liquid flows along the lower surface and vapour above. Figure 2 shows the four flow regimes that can occur in a horizontal pipe.

Several researchers have proposed several classification of micro to macro channel. In general, a microchannel is a channel for which the heat transfer characteristics deviate from predictions from widely accepted models for conventional sized channel. Mehendale et al. [7] proposed a classification based on hydraulic diameter and consider range from 1μm to 100μm as microchannel, 100μm to 1000μm as mini channel and greater than 1mm as macrochannel. Kandlikar et al. [8] also classified as similar approach. They proposed that diameter below 200μm as micro channel, from range 200μm to 3mm as mini channel and above 3mm as macro channel. Kew and Cornwell [9] proposed a confinement number, Co, as,

$$Co = \left[\frac{\sigma}{g(\rho_L - \rho_V)D_h^2}\right]^{1/2}$$

where σ is the surface tension, g is the gravitational acceleration, ρ_L and ρ_V are liquid and vapour densities of fluid respectively. D_h is the hydraulic diameter of flow channel. They showed Co=0.5 as the transition criteria from micro to macro channel. Harirchian and Garimella [10] showed that flow confinement depends not only on channel size but also on mass flux since the bubble diameter varies with flow rate. Then they proposed a new correlation, represented by,

$$Bo^{0.5} * Re = \frac{1}{\mu_f}\left[\frac{g(\rho_f - \rho_g)}{\sigma}\right]^{0.5} GD^2 = 160$$

This new flow boiling transition criteria recommends that for $Bo^{0.5} * Re < 160$, vapour bubbles are confined and the channel should be considered as microchannels.

A large number of studies have been undertaken on the topic of flow boiling heat transfer mechanism to understand the fundamental of this process (Sobhan and Garimella [11]; Thome [12]; Bertsch et al. [13]). More recent works have been attempted to better understand the flow patterns occurring during boiling in micro channel using different working fluids (Sehwan and Sangkwon [14]). Harirchian and Garimella [15] have studied the size effects on local flow boiling heat transfer to a dielectric fluid. High speed flow visualization also has been employed to understand the physics of boiling in microchannels (Chen and Garimella [16]). Flow regime map also has been proposed for microchannel (Harirchian and Garimella [10]). In spite of this large number of investigation, flow boiling in micro scale has not been fully understood.

Two-phase flow instabilities may arise when boiling occurs in conventional size channels and more so in a parallel array of multiple micro/mini-channels. These undesired effects must be controlled or mitigated because they can induce mechanical vibrations in the system, degrade the heat transfer performances (premature dryout, CHF limitation) etc. Two-phase flow instability is a complex topic because several effects may occur simultaneously and play a role in a coupled way. Two-phase flow instabilities can be classified into various types with different driving forces. From the various instabilities encountered during flow boiling, several modes appear to be important in microchannels: excursive (and parallel channel)

instability, compressible volume/pressure drop instability, rapid bubble growth, and CHF conditions.

Several reviews on the two-phase flow instabilities in conventional size channels have been compiled by Bergles [17], Ishii [18] and Yadigaroglu [19]. They presented the varied phenomena and theories available in the literature. The classical theories developed for conventional size channels can be used to a limited extent for interpreting the instabilities phenomena observed in micro/mini-channels. In fact, when dealing with phase-change phenomena the basic mechanisms such as nucleation, coalescence, fragmentation, and interfacial instabilities still exist. Nevertheless, when micro/mini-channels are involved, some differences exist. For instance, in a small size channel the vapor growth phase is limited in the radial direction because of the hydraulic diameter. Only the axial direction allows vapor growth when boiling occurs. As a result there are important differences observed in the physical processes when compared to conventional macro-scale systems. At present, parallel channel oscillations and single channel oscillations were clearly identified in narrow channels. What is typical for these geometries is the appearance of an intermittent dry out which produces a vapor recoil in the micro/mini-channel. Depending on the compressibility of the inlet zone of the channel, quasi- periodical pressure fluctuations are observed. These oscillations are due to the competition of the inertia or gravity effects and the vapor recoil pressure linked to the imposed heat flux on the wall [20]. The phenomenon characterized by vapor expansion in both the upstream and downstream directions causing flow reversal was observed by Kandlikar et al. [21] and also by Kandlikar and Balasubramanian [22]. They employed a high-speed digital video camera to observe this behavior. Similar instabilities were observed by Hetsroni et al. [23] and Peles [24], among other investigators. Kuo and Peles [25] studied the pressure effect on flow boiling instabilities in microchannels. They showed that at high pressure at a given mass quality reduces the void fraction, the low superheat needed to activate bubble nucleation during flow boiling. Flow visualization revealed smaller bubble departure diameters at high system pressure. The reduction of bubble departure diameter is an indicative of reduced rapid bubble growth oscillation. Local transient temperature measurements showed lower magnitudes and higher frequencies of oscillations at high system pressure. The higher frequencies may be linked to density wave instability and can result in low temperature oscillation magnitude. The rapid bubble growth accompanied by the fluctuations in pressure drop introduces instabilities in the two phase flow boiling in

mini/ micro-channels. This condition has negative effects on the heat transfer performance. At present, the local reversed flow phenomenon is not well understood and not well studied.

Only a few attempts have been reported to control it. Kandlikar et al. [26] conducted experiments to study the instability observed during flow boiling in micro-channels and concluded that artificial nucleation sites, fabricated by laser micromachining, as shown in Figure 3, in conjunction with the 4% area pressure drop elements completely eliminated the instabilities associated with the reverse flow.

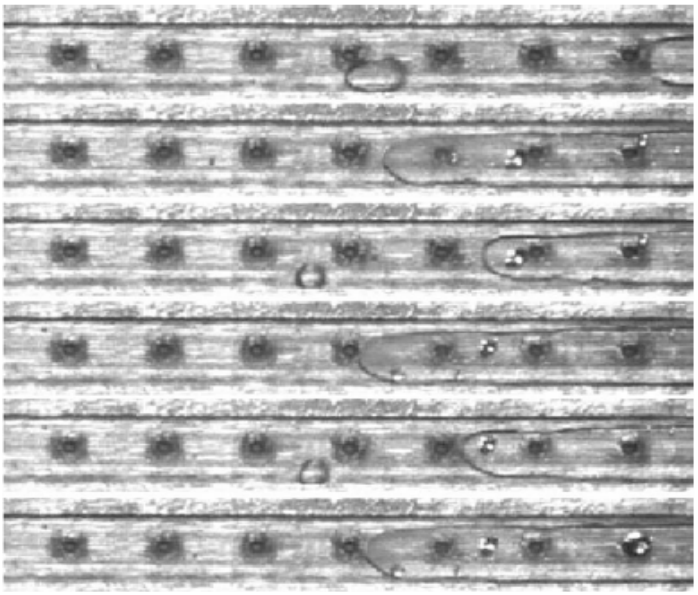

Figure 3: Fabricated nucleation sites [26].

Lu and Pan [27] explored experimentally stabilizing flow boiling of water in ten parallel microchannels on a heat sink with a diverging cross-section design as shown in Figure 4. Each diverging microchannel had a mean hydraulic diameter of 120 μm and a diverging angle of 0.5° while the channel depth is uniform at 76 μm. They concluded that in terms of stability performance, the flow boiling in the parallel microchannel heat sinks with a diverging cross-section design is superior to a uniform cross-section design. They discussed that conceivably, a larger diverging angle will help resisting the reversed flow of vapor bubbles. However, a larger diverging angle also slows down the flow velocity and may cause more intensive boiling or evaporation and even trigger the dryout, especially near the exit.

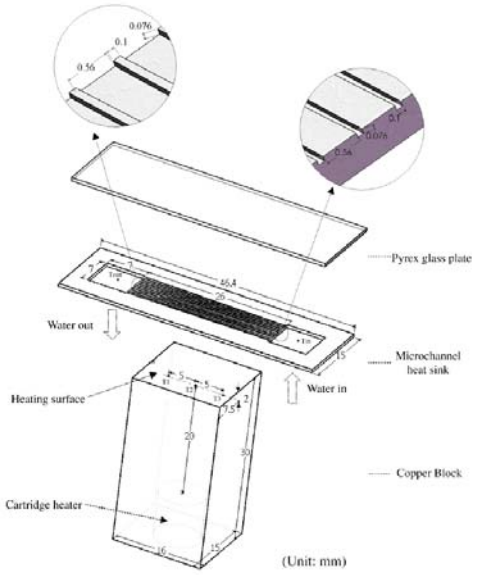

Figure 4: Micro-channel heat sink with diverging cross-section design [27].

Qu [28] introduced an improved micro-channel heat sink with cross connections in the transverse direction as shown in Figure 5. He claimed that the cross-connected micro-channel heat sink enabled a uniform pressure field to be maintained for the two-phase flow boiling of liquid coolant in the heat sink. The cross connection design prevents the severe flow oscillation that can occur in parallel channel designs due to feedback interaction between flow channels through common inlet and outlet plenums, by promoting the communication of flow between the channels and creating a uniform pressure field in the heat sink.

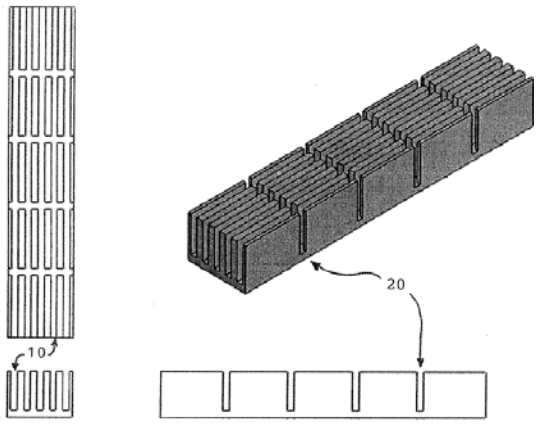

Figure 5: Cross-connected micro-channel heat sink [28].

The heat generation from chips increases rapidly with the evolution of integrated circuit technology. Furthermore, the problem of hotspots within a given chip, where local heat

generation rates far exceed the average on the chip, strongly increases the peak temperature for a given total power generation. Hotspots imposed by spatially non-uniform heat flux in a high performance circuit increase the chip maximum junction temperature, which degrades the reliability and performance of electronic equipments. More aggressive cooling solutions are required to reduce temperatures near hotspots, whose temperatures can be minimized through tailored heat sink solutions. Only a few attempts have been reported to mitigate hotspots on chips. Jae-MO Koo et al. [29] theoretically examined the heat transfer and fluid flow characteristics of two-phase flow in microchannels with hydraulic diameters of 150 - 450 micrometers for strongly varying wall heat flux conditions. The theory developed aims to help minimize the pressure drop in the two-phase region and to provide the foundation for optimizing channel dimensions to reduce temperature variations. Their results indicated that the optimal thermal configuration is to apply higher power near the exit region since it minimizes the pressure drop of the two-phase flow field and the corresponding wall temperature. Eun Seok Cho et al. [30] proposed a cross-linked microchannel heat sink and claimed to achive better cooling performance due to the lateral fluid transport and mixing.

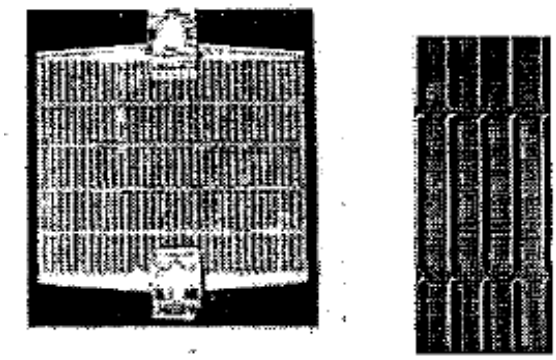

Figure 6: Cross-linked microchannel and cross-linked section [30].

To handle the high power dissipation and extremely high heat flux associated with next generation of electronics, liquid or two-phase microchannel cooling solutions need to be considered. However, in order to improve the efficacy of advanced, liquid or two-phase cooling solutions, the thermal performance of the thermal interface materials (TIM) must be further improved. Alternatively, the challenging but more attractive solution would be to use two-phase microgap channel coolers [31-34] to directly cool the heat sources. Microgap coolers provide direct contact between chemically inert, dielectric fluids and the back surface of an active electronic component, thus eliminating the significant interface thermal resistance associated with Thermal Interface Materials and/or solid-solid contact between the

component and a microchannel cold plate. The exploratory study of the thermofluid characteristics of two-phase microgap coolers by Kim et al. [32] revealed that the intermittent and annular flow regimes dominate the behavior of 110μm to 500μm channel behavior for the the two-phase flow of FC-72, with a liquid volumetric flow rates from 0.17ml/s to 0.83ml/s and area-averaged heat transfer coefficients as high as 15.5 kW/m^2-K can be attained. In addition the two-phase microgap channel coolers can potentially address the flow instabilities and flow reversal issues inherent with two-phase microchannel heat sinks. Bar-Cohen and Rahim [5] performed a detailed analysis of microchannel/microgap heat transfer data for two-phase flow of refrigerants and dielectric liquids, gathered from the open literature and sorted by the Taitel and Dukler flow regime mapping methodology and found annular flow to be the dominant regime for this thermal transport configuration and to grow in importance with decreasing channel diameter. Sheehan and Bar-Cohen [34] studied wall temperature fluctuation in two phase flow of a 210 micron microgap channel, operated with mass flux of 195.2 kg/m^2-s and subjected to heat flux varying from 10.3 to 26 W/cm^2. These temperature fluctuations were found to vary independently with both the thermodynamic quality of the flow and the wall heat flux. As the concept of two-phase microgap channel cooler is still very new, more work should done to advance the fundamental understanding of the underlying mechanism(s).

3. Experiments

3.1 Experimental Setup

The experimental flow loop consists of a Stainless steel reservoir (Portable Wide Mouth ASME 01 EA Pressure Tank 304 SS) of 3 gallons capacity to store Deionized water. Two cartridge heaters (600Wx2) fitted into the reservoir was used to boil the water for degassing purpose. Deionized water was pumped through the flow loop using a gear pump (Cole Parmer Bench Top Analog Drive EW-74013-65). The fluid first encounters an inline 15 µm filter (Swagelok SS-4FW-15) to remove impurities. Flow rate was measured using a Mcmillan Liquid flow sensor (Model 106-5-D-T4-C6-HT) which has a maximum operating temperature of 85 °C. After flowing through the flow sensor the deionized water was preheated by hot water from a water bath circulated through a compact liquid-to-liquid heat exchanger before entering the test section. Temperature measurements were done before entry into the heat exchanger, after exiting the heat exchanger, at the inlet and outlet of the test section using type-T thermocouples from Watlow. The inlet and outlet pressure were measured using Huba Pressure transmitter (Model: 507.910013111) having a range of 0 to 0.6 bar. The preheated water then enters the test section containing the microgap heat sink. Constant-voltage power is supplied to the integrated heaters on the backside of the chip to provide the desired heat flux for the flow boiling experiment. Water enters the microchannels as single-phase liquid and first heats up to its saturation temperature before undergoing phase change. Holes are drilled into the top cover of the test section for locating the pressure taps and thermocouples. These taps are positioned as close as possible to the microgap. The temperature distribution on the chip is measured using an integrated 5x5 diode temperature sensor array. Hot water exiting the test section was cooled using a Thermatron liquid-to-air heat exchanger (Model 735SPC0A01) before flowing back into the reservoir. Swagelok Stainless Steel pipes and fittings were used to construct the flow loop. The data from all different sensors were collected using a computer- based Data acquisition and measurement control system Agilent 34980A Multifunction Switch/Measure Unit and typical plug-in modules. Figure 7(b) shows the actual experimental setup.

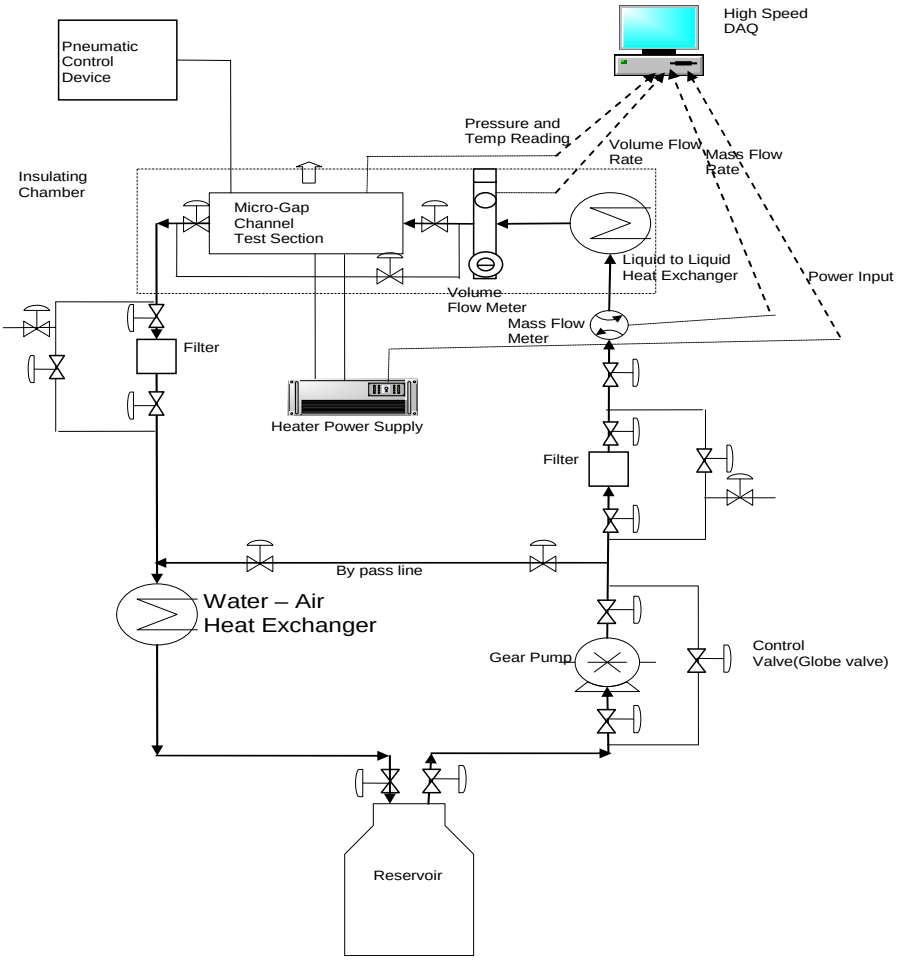

Figure 7(a): Proposed Flow Loop.

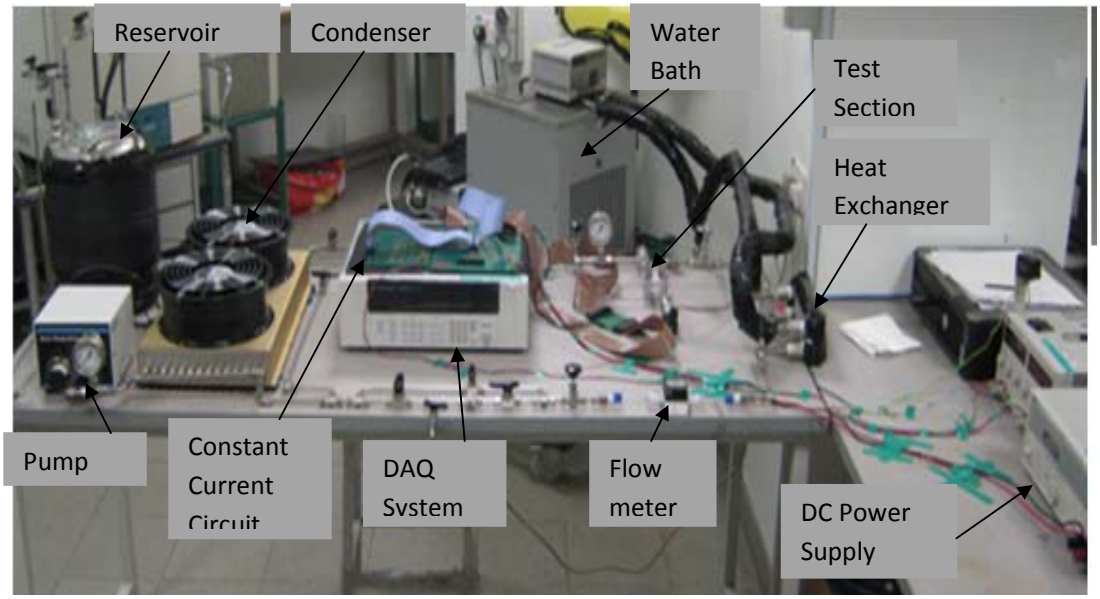

Figure 7(b): Experimental Setup.

3.2 Test Section

The test section consists of a silicon microgap test piece, a top cover and a base plate as shown in Figure 8(a). The microgap test piece is fabricated from a test chip which includes a 5 x 5 array of heat sources and temperature-sensing diodes as shown in Figure 8(c). A numbering scheme for the 25 heaters/ temperature sensor elements is also indicated in the figure.

Each of the 25 heater/temperature sensor elements is 2.54 mm x 2.54 mm in size and incorporates a heating element and integrated diode sensors for on-die temperature monitoring. Resistive heating in the die is accomplished by driving a current through doped silicon well between a pair of bus bars. At the top and bottom of the die is a pair of pads which connect a serial five-diode temperature sensor network [35]. The thermal test dies are fabricated using a five-inch type-P silicon wafer with orientation 111. The dies are 625 μm thick and are diced in arrays of 5 x 5, resulting in chips of dimension 12.7 mm x 12.7 mm. The diced chips are mounted on printed circuit boards (PCB) using 63Sn/ 37Pb solder bumps. Table 1 includes the dimensions (measured) of the microgap and the test conditions used. A transparent (a type of polycarbonate) cover is used over the test piece to make microgap and to provide the plumbing connections. Appropriately designed inlet and outlet manifolds are formed within this cover to minimize the flow mal-distribution across the heat sink. Taps are included for the inlet and outlet pressure transducers and thermocouple probes. A square O-ring seals the test piece between the cover and the chip to ensure good sealing of the microgap. The test section is assembled by bolting at the four corners as shown in Figure 8(d).

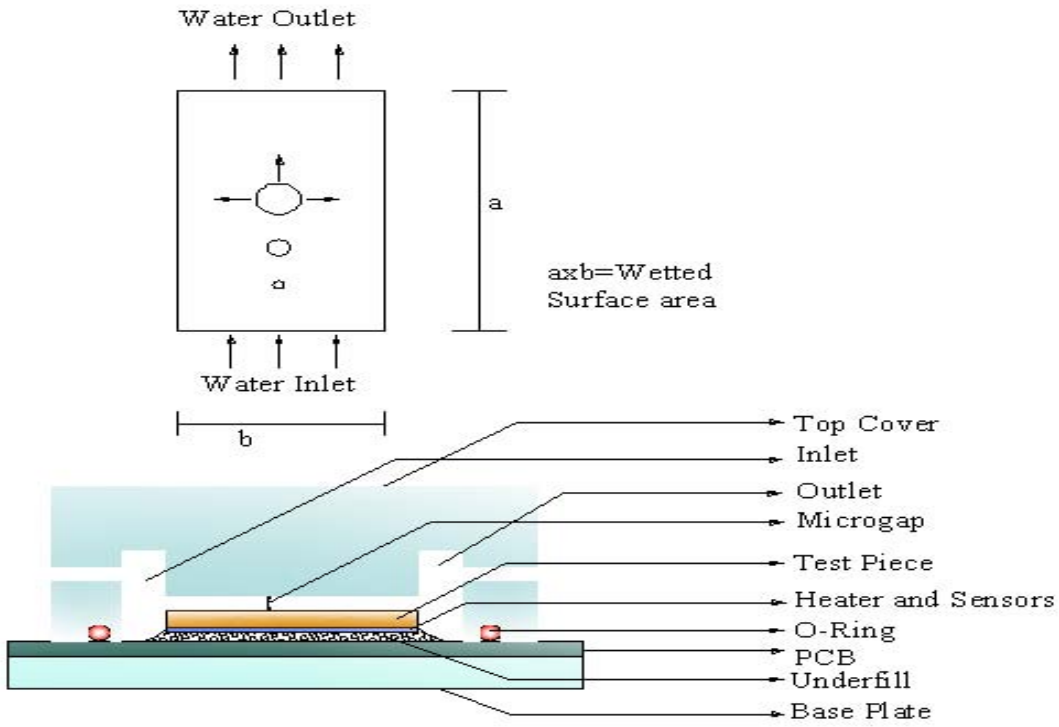

Figure 8(a): Schematic diagram of Microgap Test Section.

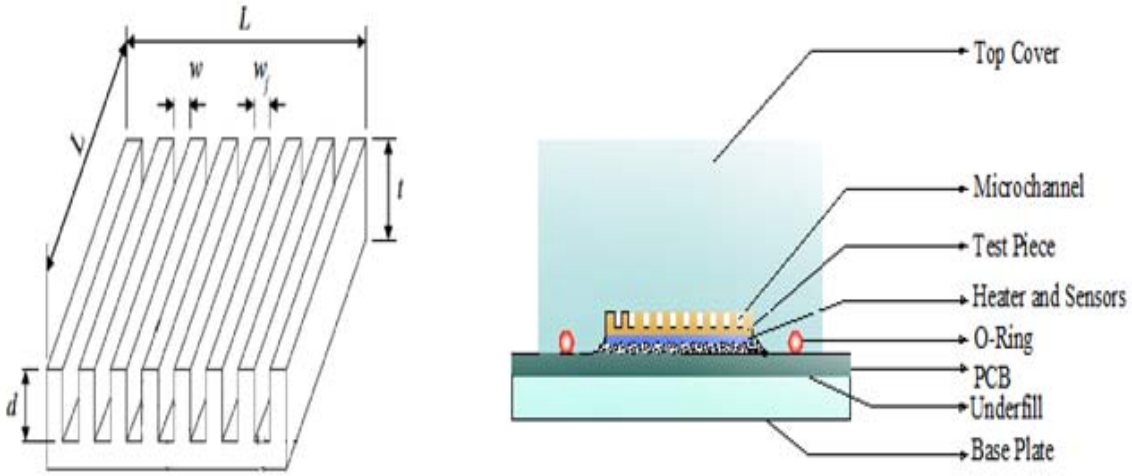

Figure 8(b): Schematic diagram of Microchannel Test Section.

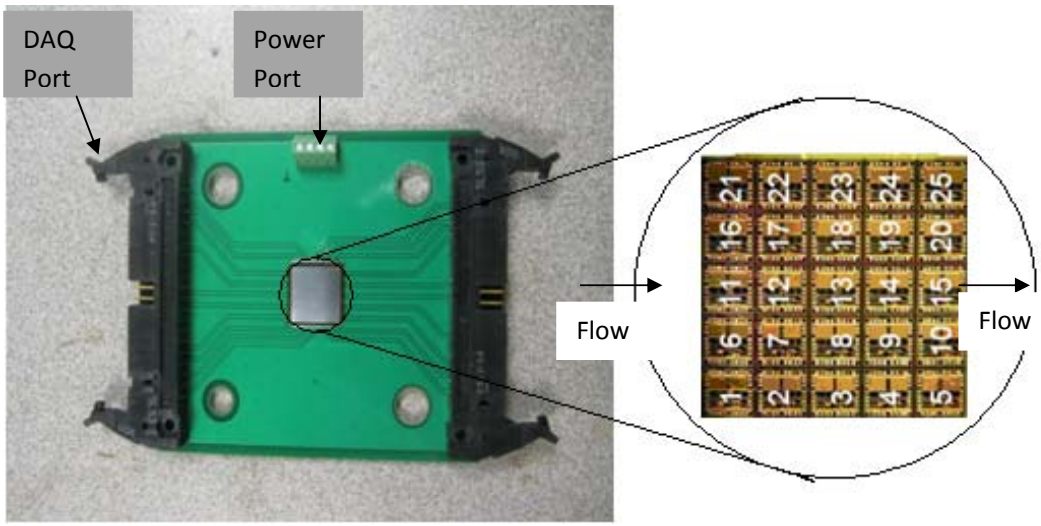

Figure 8(c): Test piece with 5 x 5 array of heating elements and integrated diode temperature sensors.

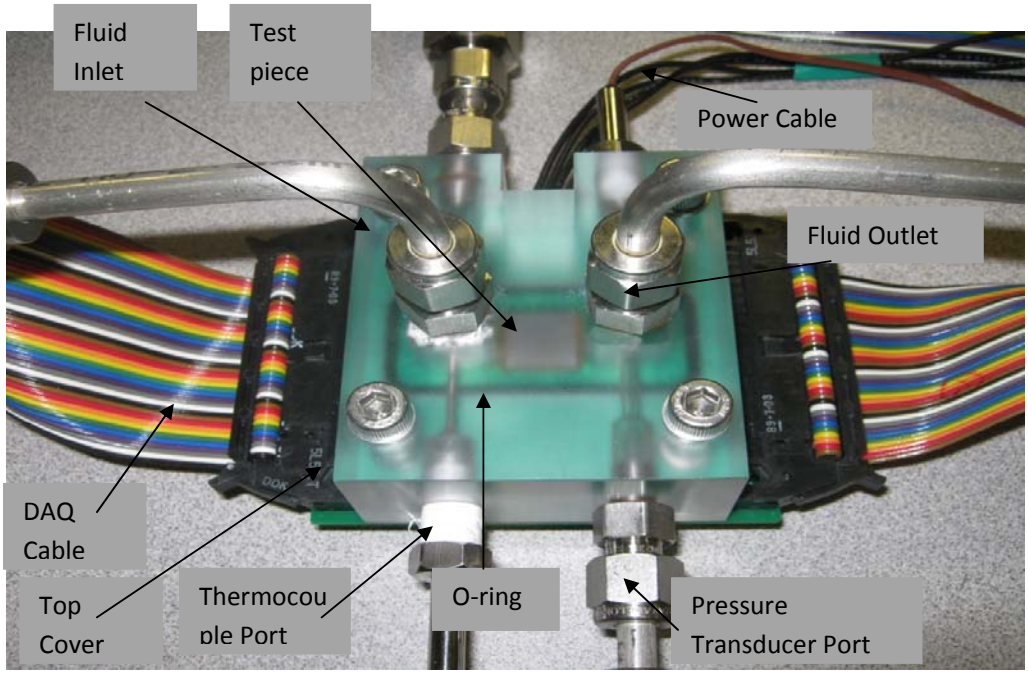

Figure 8(d): Microgap test section.

Test matrix used for flow boiling pressure drop and heat transfer study in microgap:

Table 1

Case	Length, L (mm)	Width, W (mm)	Gap Height, H (μm)	G (Kg/m²s)	$T_{f;i}$(˚C)	q_{eff} (W/cm²)
1.1	12.7	12.7	190	420	86	0-100
1.2	12.7	12.7	190	690	86	0-100
1.3	12.7	12.7	190	970	86	0-100
2.1	12.7	12.7	285	420	86	0-100
2.2	12.7	12.7	285	690	86	0-100
2.3	12.7	12.7	285	970	86	0-100
3.1	12.7	12.7	381	420	86	0-100
3.2	12.7	12.7	381	690	86	0-100
3.3	12.7	12.7	381	970	86	0-100

Test matrix used for flow boiling pressure drop and heat transfer study in microchannel:

Table 2

Case	Length, L (mm)	Channel Width, w (μm)	Channel Depth, d (μm)	No. of channel	G (Kg/m²s)	$T_{f;i}$(˚C)	q_{eff} (W/cm²)
1.1	12.7	208.28	385.70	30	420	86	0-100
1.2	12.7	208.28	385.70	30	690	86	0-100
1.3	12.7	208.28	385.70	30	970	86	0-100

3.3 Silicon Diode Temperature Sensor Calibration

Before the diode temperature sensors can be used for temperature measurement, their voltage–temperature response is characterized through calibration. The calibration is performed in a convection oven over temperature settings from room temperature to 90˚C, in steps of 10˚C. When the temperature in the oven reaches each desired steady-state value, typically in 30–40 min, the voltage drop across each diode is recorded. By correlating the voltage drop to temperature, the temperature response of each diode can be established as is illustrated in Figure 9. This response is clearly seen to be very linear.

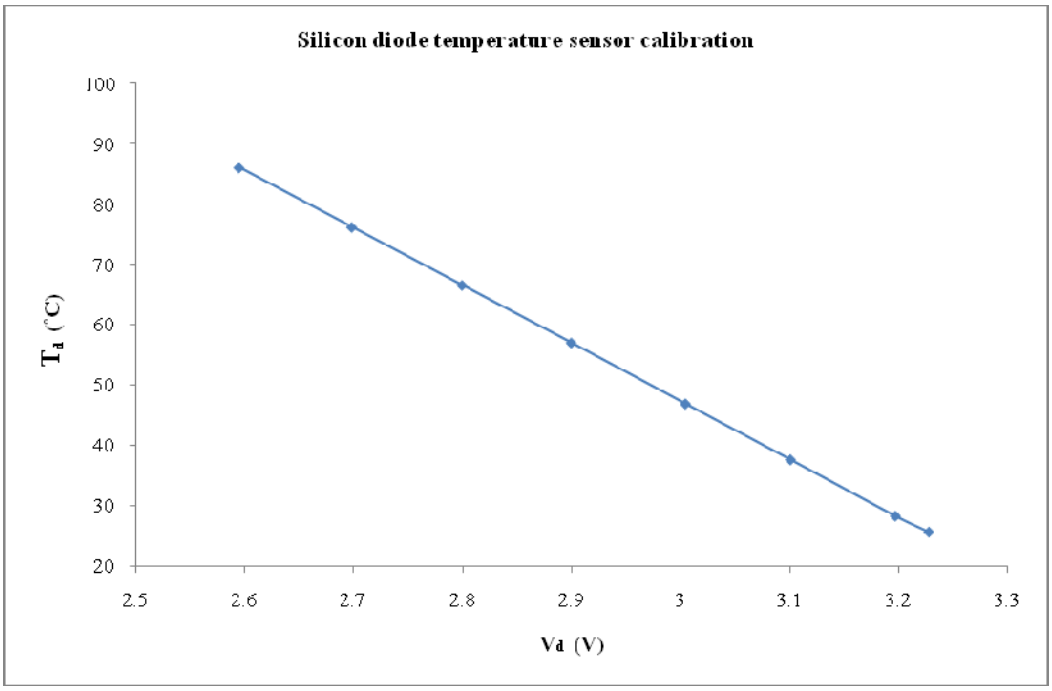

Figure 9: Typical calibration curve of silicon diode temperature sensor.

3.4 Heat Loss Characterization

To establish the fraction of the total heat input that is dissipated via the flow boiling process, heat losses via other paths, i.e., natural convection, radiation, and conduction via the PCB, are experimentally determined as follows. The test piece is first completely drained of water. The chip is then heated by applying a constant voltage source to the heaters. A steady state is reached after about 20–30 min in these heat loss tests, at which time readings from all diode temperature sensors are within ±0.1 ˚C. The temperature readings from the 25 diodes are then recorded over a 2-min period and averaged. Tests are repeated for different levels of input power. The average diode temperature is then correlated to the input power and a linear

relationship is obtained as shown in Figure 10. This relationship, $q_{loss} = 0.1065T_{d,avg} - 2.6746$, is then used during the flow boiling experiment to account for the heat losses.

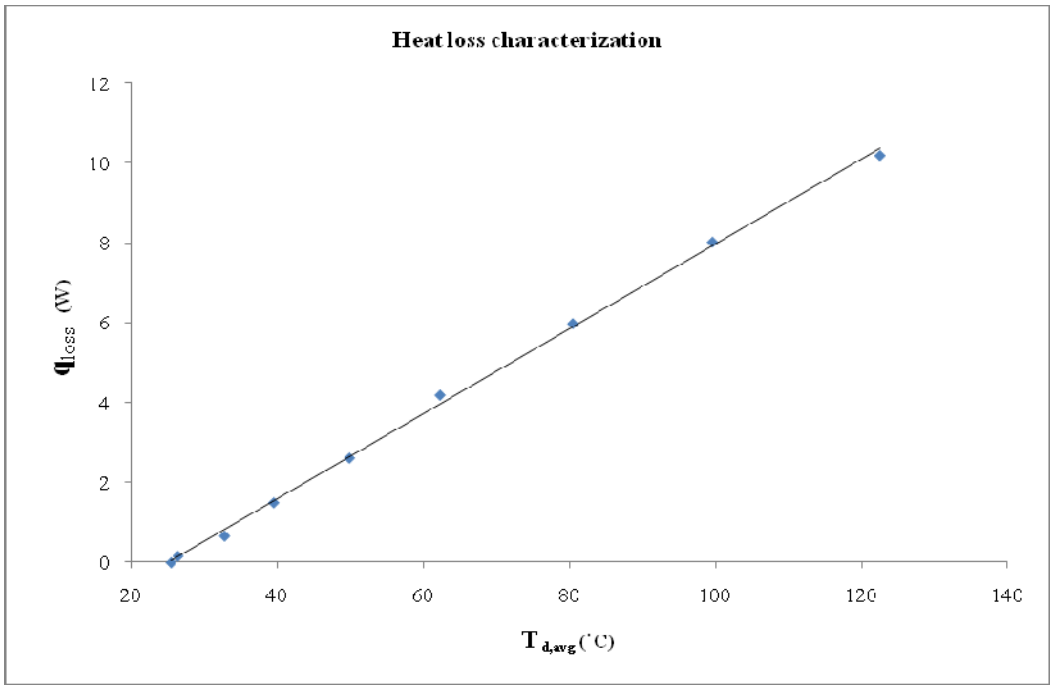

Figure 10: Heat loss characterization.

To verify this heat loss analysis, the relation $q_{loss} = q_{supply} - \dot{m}_{water} c_p \Delta T$, is used. The average diode temperature is then correlated to this calculated heat loss data and a linear relationship is obtained. The heat loss data without water and with water in single phase region are compared in Figure 11and the difference is found to be within 15%.

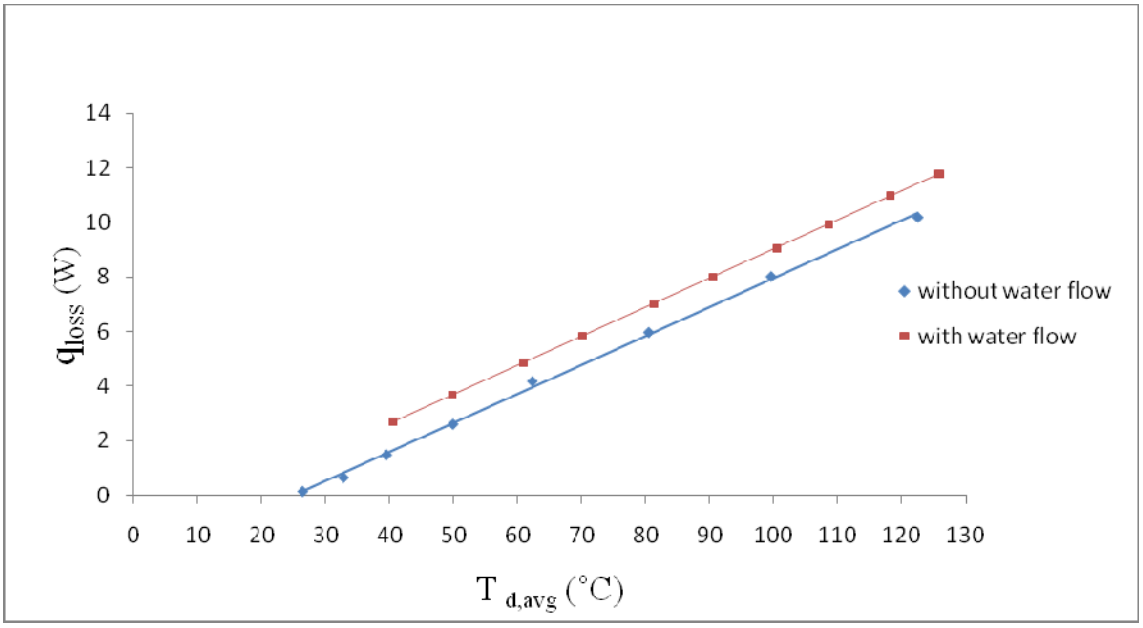

Figure 11: Heat loss comparison.

3.5 Experimental Procedure

The fluid is degassed prior to each experimental run. Degassing is conducted by boiling the water in the reservoir vigorously using two imbedded cartridge heater (600Wx2 for one and half hour. Ventilation is made at the top of the reservoir to remove dissolve gases. The dissolved oxygen (DO) content at the end of this degassing process is around 3.94 ppm, as measured by a DO sensor. In each experiment, the power supply to the heaters is set to the desired value after the flow rate and the inlet fluid temperature are stabilized. Steady state is reached after about 20–30 min in each test run, when all temperature readings are within ±0.5 °C for about 2 min. All power, temperature, pressure and flow rate measurements are averaged over a 2 min period. The heat flux is then increased for the next test, in increments of 10W/cm², and the experimental procedure repeated.

Experiments were conducted at mass flux ranging from 420 Kg/m²s to 970 Kg/m²s and inlet water temperatures 86°C, for effective heat flux up to 100 W/cm².

3.6 Data Reduction

3.6.1 Pressure Drop Data Reduction

As the pressure taps are located upstream and downstream of the microgap and microchannel in the inlet and outlet plenum, the measured pressure drop includes the sum of pressure drops across the bends from inlet plenum to the inlet manifold and from outlet manifold to the outlet plenum and the pressure loss and recovery resulting from the inlet contraction and outlet expansion, apart from the frictional drop across the microgap and microchannel. Calculations were made based on the methods described in [36] and [37] and it was identified that the other pressure losses apart from the frictional drop were less than 5% of the total pressure drop and hence were neglected. Therefore, the pressure drops reported below were obtained directly from the sensors.

$$\Delta P_{gap} = P_i - P_o \quad \text{..... (1)}$$

$$\Delta P_{channel} = P_i - P_o \quad \text{..... (2)}$$

3.6.2 Heat Transfer Data Reduction

The heat transfer rate to the fluid in the microgap and microchannel is obtained by subtracting heat loss from the input power:

$$q_{eff} = q - q_{loss} \quad \text{..... (3)}$$

where q_{loss} is computed as explained in the earlier section. For the range of conditions considered in this study, over 90% of the input power is transferred to water once boiling commences in all the experiments.

The associated effective heat flux q_{eff}'' is calculated based on the footprint area of the heater which is same as the base of the microgap heat sink, $A=W \times L$. This is also the reported heat flux that the heat sink can dissipate:

$$q_{eff}'' = q_{eff}/A \quad \text{..... (4)}$$

For microchannel, the total wetted area of the microchannels is:

$$A_c = N(w + 2nd)L \quad \text{..... (5)}$$

where N is total number of channels; w , d and L are the width, depth and length of the channel respectively and η is the efficiency of a fin with adiabatic tip which is correlated by:

$$\eta = \frac{\tanh(md)}{md} \quad \text{..... (6)}$$

and

$$m = \sqrt{\frac{2h}{K_s w_w}} \quad \text{..... (7)}$$

So, the associated effective heat flux $q_{1}eff^{1}$ in microchannel is calculated by:

$$q_{1}eff^{1} = q_{1}eff/A_{1}c \quad \text{.....} \quad \text{(8)}$$

Water was supplied into the heat sink in a subcooled state ($T_{f,i} < T_{sat}$) for all test conditions. The microgap can therefore be divided into two regions: an upstream subcooled inlet region and a downstream saturated region; the location of zero thermodynamic equilibrium quality ($x = 0$) serves as a dividing point between the two regions. The length of the two regions can be evaluated from,

$$L_{1}sp = (m'c_{1}(p(T_{1}(sat, 0) - T_{1}(f, i)))/(q_{1}eff^{1} W) \quad \text{.....} \quad \text{(9)}$$

and

$$L_{sat} = L - L_{sp} \quad \text{.....} \quad \text{(10)}$$

where $T_{sat,0}$ is the saturation temperature at the location where $x = 0$. In the present study, $T_{sat,0}$ is evaluated using the measured inlet pressure, P_i as pressure drop across the subcooled region is small. Eqs. (9) and (10) indicate as the heat flux increases for a constant mass flow rate, L_{sat} increases at the expense of L_{sp} .

The local heat transfer coefficient in microgap is determined from,

$$h_{1}z = (q_{1}eff^{1})/(T_{1}(w-) T_{1}f) \quad \text{.....} \quad \text{(11)}$$

The local heat transfer coefficient in microchannel is determined from,

$$h_z = \frac{q_{eff}}{A_c(T_w - T_f)}$$ …… (12)

in which T_f is the fluid temperature as defined by

$$T_f = T_{f,i} + \frac{q''_{eff} W z}{\dot{m} c_p}$$ (Single-phase region)…… (13)

$T_f = T_{sat}$ (Saturated region)..... (14)

T_w , is the local wall temperature which can be obtained by assuming one dimensional heat conduction through the substrate

$$[T]_w = T_d - (q_{eff}'' t)/K_s$$ (for microgap)…… (15)

$$[T]_w = T_d - (q_{eff}'' (t - d))/K_s$$ (for microchannel)…… (16)

where T_d is the temperature of the diode at position 15, which is the location last downstream along the center row (as shown in Fig. 8(c)). All the heat transfer results presented in this work are based on this position in the microgap heat sink as it corresponds to the second greatest degree of saturated boiling.

The exit quality is calculated from energy balance. The power supplied to the channel is used in heating the fluid up to the saturation temperature and also as latent heat during phase change. The exit quality is therefore given by,

$$[x]_{exit} = (q_{eff}'' A - \dot{m} c_p (T_f(sat, 0) - T_f(f, i)))/(\dot{m} h_{fg})$$ …… ……..... (17)

3.7 Experimental Uncertainties

The uncertainties in individual temperature measurements are ±0.5 °C for the T-type thermocouples and the diode temperature sensors employed. The measurement error for the flow meter is ±1% of full scale and that of the inlet and outlet pressure transducer is ±0.3% of full scale. The uncertainty associated with the heat flux measurement is estimated to be ±2%. The error in gap dimension measurement is ±3%. The uncertainty associated with the pressure drop measurements varied from 4%-18%. A standard error analysis as mentioned in [38] revealed uncertainties in the reported heat transfer coefficients to be 12%.

The general expression for propagation of errors:

The general expression for F=F(x, y, z) where x, y and z are independent measured values is given by,

$$\Delta F = \sqrt{\left(\left[\frac{\partial F}{\delta x}\Delta x\right]\right)^2 + \left(\left[\frac{\partial F}{\partial y}\Delta y\right]\right)^2 + \left(\left[\frac{\partial F}{\partial z}\Delta z\right]\right)^2} \quad \text{..... (18)}$$

where Δx, Δy and Δz are the uncertainties of x, y and z respectively.

4. Results and Discussion

4.1 Characteristics of Two-phase Flow and Heat Transfer Processes in Microgap Channel

4.1.1 Effect of Dimension

4.1.1.1 Boiling Curve

The effect of microgap size on boiling curve for mass flux 420kg/m²s is shown in Figure 12. The onset of boiling can be identified in the figure as the point where the wall temperature exhibits a sudden change in slope from its single-phase dependence. At low heat fluxes, the slopes of all boiling curves are fairly constant, indicative of single-phase heat transfer while in the two-phase region, a modest rise of wall temperature can be seen for the further increment of heat flux. After the onset of nucleate boiling, the wall temperature shows a weak dependency on heat flux for all gap size. This shows the dominancy of nucleate boiling flow regime. As further increase of heat flux at around 40W/cm², the wall temperatures become dependent of heat flux and the boiling curves deviate for different gap size shows the convective boiling dominance. For low mass flux like 420kg/m²s, all the microgap size shows almost the similar characteristics and with the increase of heat flux, the wall temperatures also increase. This strong dependence of the wall temperature on the heat flux for these microgap size at low mass flux indicate that convective boiling rather than nucleate boiling, are the main heat transfer mechanisms.

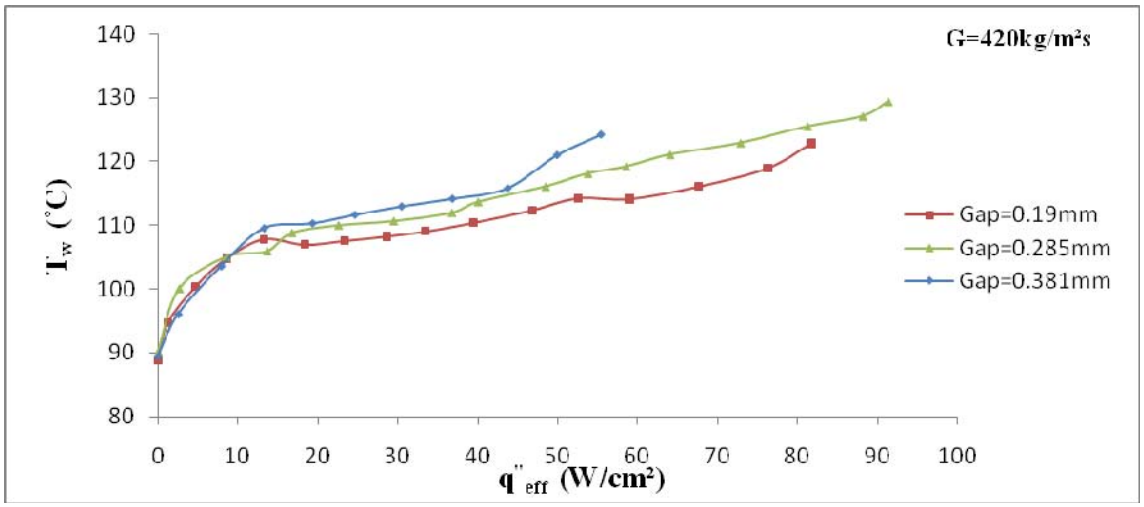

Figure 12: Effect of microgap dimensions on local wall temperatures at G=420kg/m²s.

For higher mass flux like 690kg/m²s and 970kg/m²s, the smaller microgap size shows more dependency of wall temperature on heat flux rather than higher gap size. This phenomenon may happen due to confinement effect as gap size was reduced below the bubble departure diameter. This reveals that thin film evaporation and convective boiling is the main heat transfer mechanism rather than nucleate boiling in small microgap size. As convective boiling is the main heat transfer mechanism in lower gap, it transfers more heat and maintain lower wall temperature. This can be seen in Figures 13 and 14.

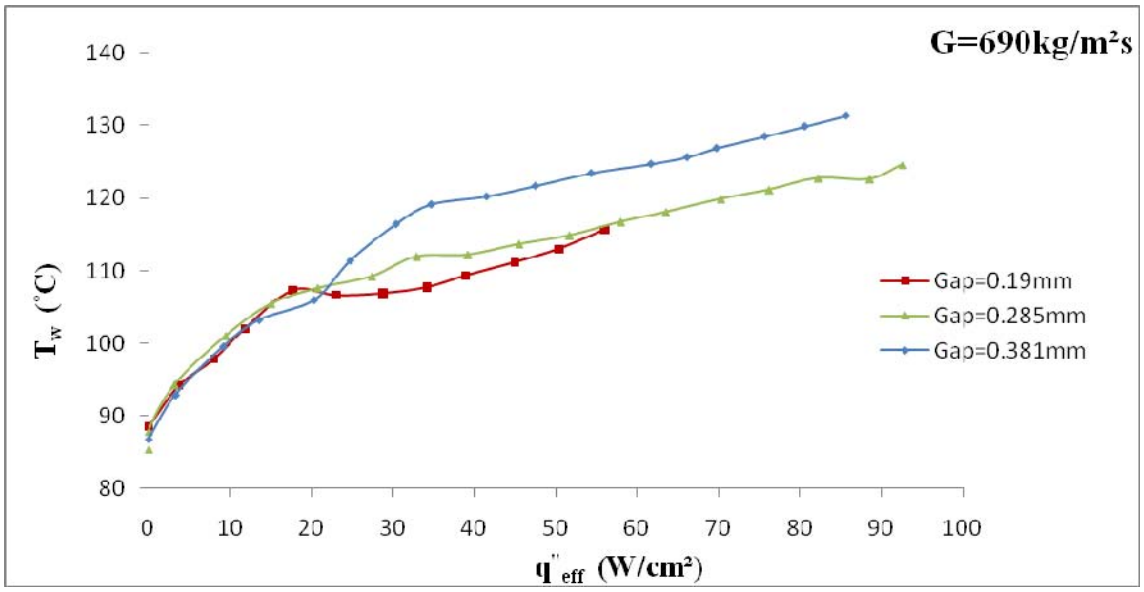

Figure 13: Effect of microgap dimensions on local wall temperatures at G=690kg/m²s.

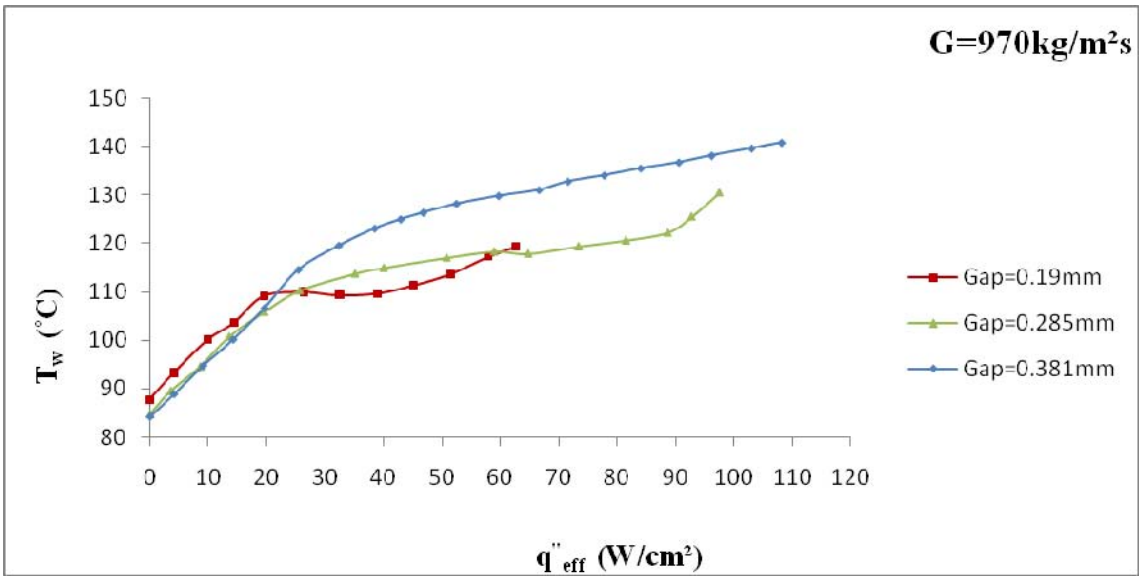

Figure 14: Effect of microgap dimensions on local wall temperatures at G=970kg/m²s.

4.1.1.2 Local Heat Transfer Coefficient

The effect of microgap size on local heat transfer coefficient is shown in Figure 15. The local heat transfer coefficient is calculated at position 15, the central diode in the last downstream location as indicated in Figure 8(c). The presence of local temperature sensors allows the local heat transfer coefficients to be computed. For low heat fluxes, the local heat coefficient increases almost linearly with heat flux. At higher heat fluxes, the curve shows a change in slope after the ONB as the heat transfer coefficient increase rapidly after boiling commences. For lower mass flux like 420 kg/m²s, the local heat transfer coefficient is increased with decreasing the microgap size. Due to the smaller microgap size relative to the bubble diameter at departure, bubbles occupy the microgap creates confinement effects. This confinement effect gives the higher local heat transfer coefficient for smaller microgap size. In small microgap size, bubble nucleation at the walls is not the only heat transfer mechanism, and the evaporation of this liquid film at the walls in the slug and annular flows also contributes to the heat transfer. Therefore, the value of local heat transfer coefficient is larger for this smaller gap. The heat transfer coefficient starts to decrease at around 50-60 W/cm². This may be due to partial dryout that happen in microgap wall with higher heat flux.

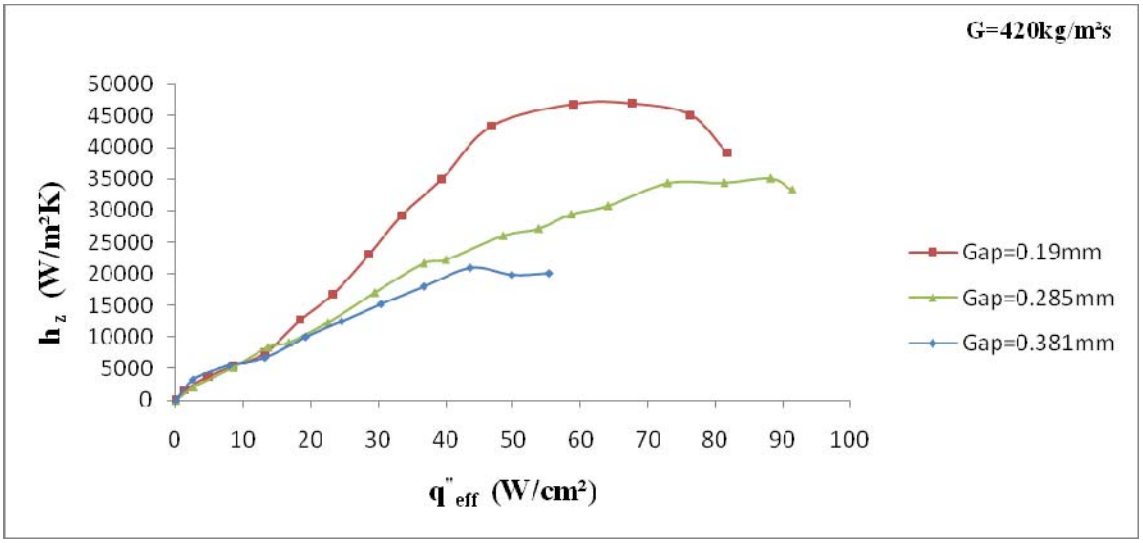

Figure 15: Effect of microgap dimensions on local heat transfer coefficients at G=420kg/m²s.

For higher mass flux like 690 kg/m²s and 970 kg/m²s, the local heat transfer coefficient shows a similar characteristic as 420 kg/m²s as shown in Figures 16 and 17. But compare to lower mass flux, heat transfer coefficient starts to decrease at lower heat flux in higher mass flux. This result can be explained in the view of fact that at a given mass flux, with the decrease of microgap size, the heat transfer coefficient increased until it reached a maximum, after which it deteriorated with decreasing gap size as CHF values and boiling data show deteriorated performance [39]. From boiling curve, it can be seen that for high mass flux in smaller microgap size, boiling data is deteriorated. Therefore, at higher mass flux, for smaller gap size, the heat transfer coefficient is lower since partial dry out occurs very early.

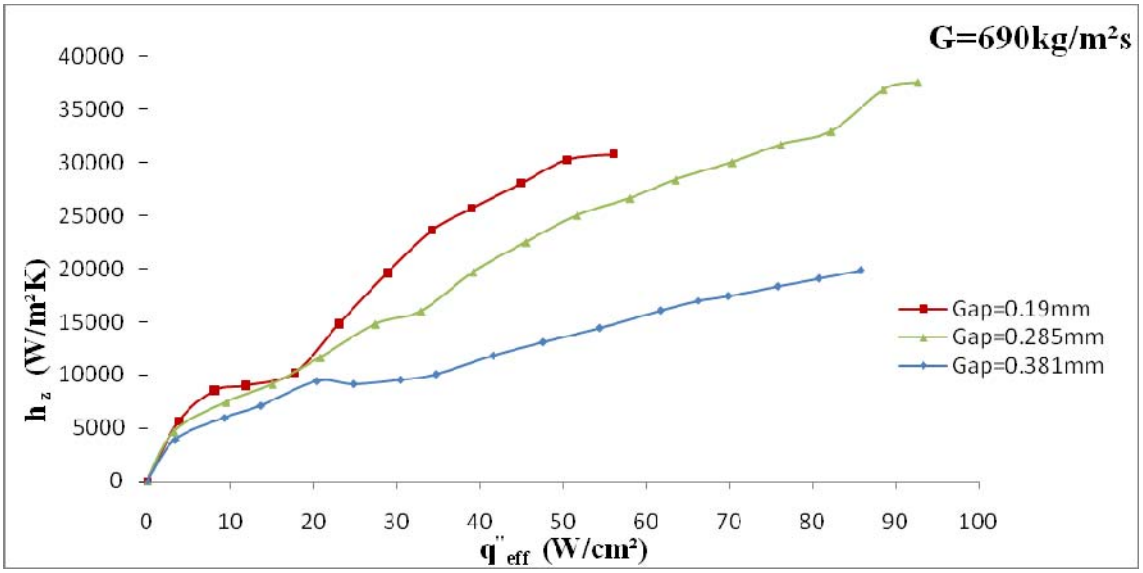

Figure 16: Effect of microgap dimensions on local heat transfer coefficients at G=690kg/m²s.

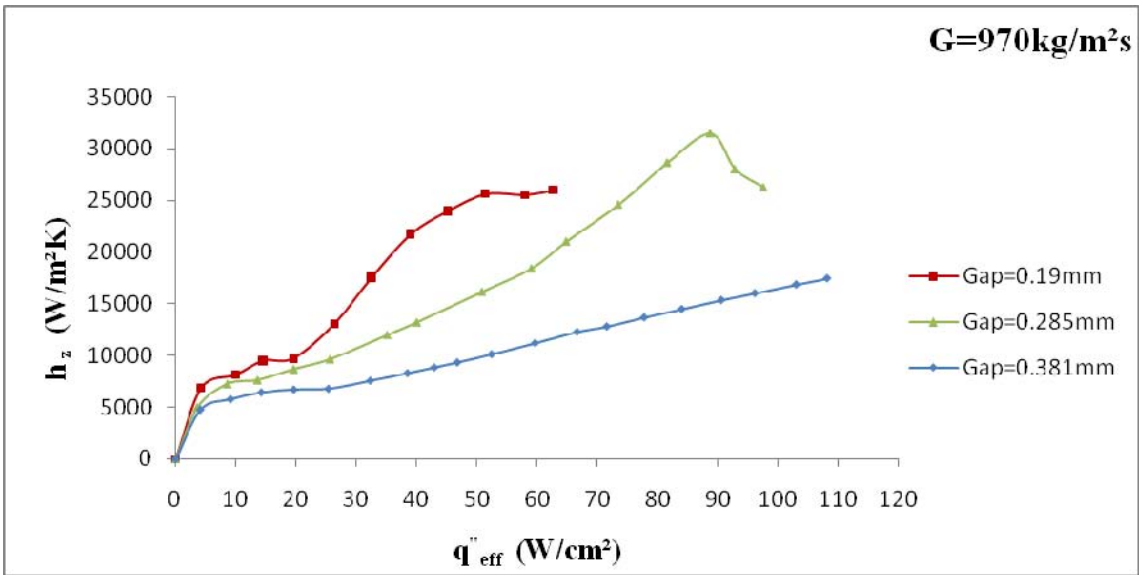

Figure 17: Effect of microgap dimensions on local heat transfer coefficients at G=970kg/m²s.

4.1.1.3 Pressure Drop

Figure 18 presents the measured pressure drop between inlet and outlet of the microgap as a function of effective heat flux for water mass flux G=420 kg/m²s for different microgap sizes. In the single phase region, pressure drop decrease slightly with increasing heat flux as the fluid viscosity decreases with the increase in temperature of the fluid. In the two phase

region, the pressure drop increases with increasing heat flux as vapour content increase with the increase in temperature of the fluid. When the effective heat flux is exceeded onset of nucleate boiling, the pressure drop increase with heat flux as the acceleration effect of the generated vapor becomes pronounced. The pressure drop increases with decreasing the microgap size. But for all mass fluxes and gap sizes, pressure drop is very low comparative to other micro channels [15].

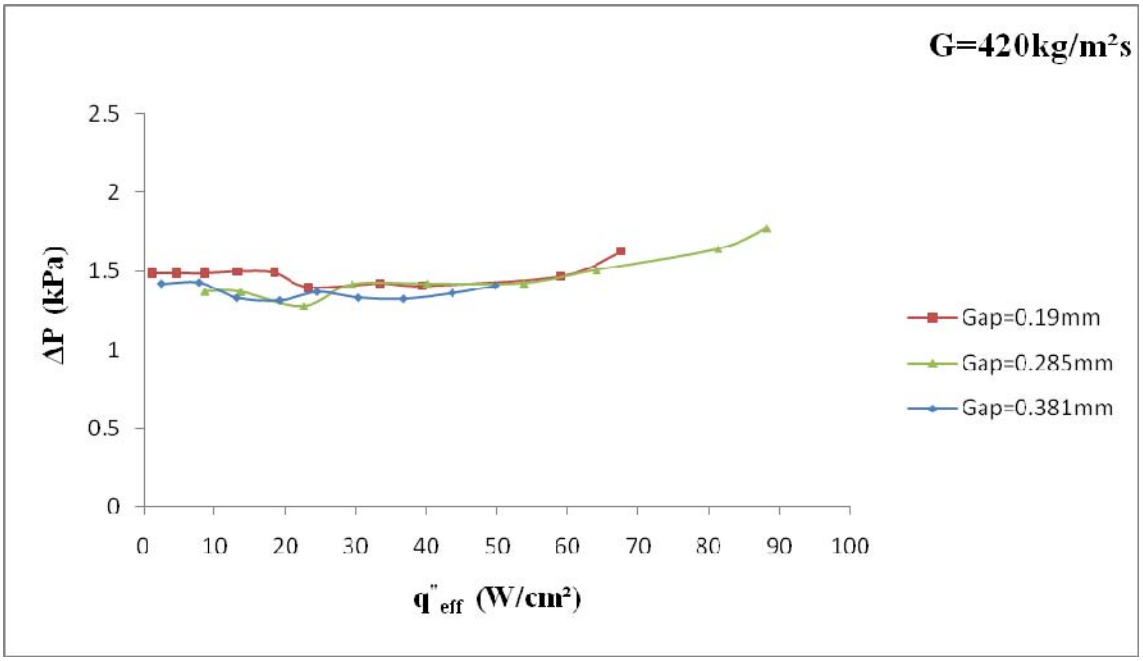

Figure 18: Effect of microgap dimensions on pressure drop at G=420kg/m²s.

Similar phenomenon has been observed for higher mass flux of 690 kg/m²s and 970 kg/m²s as shown in Figures 19 and 20.

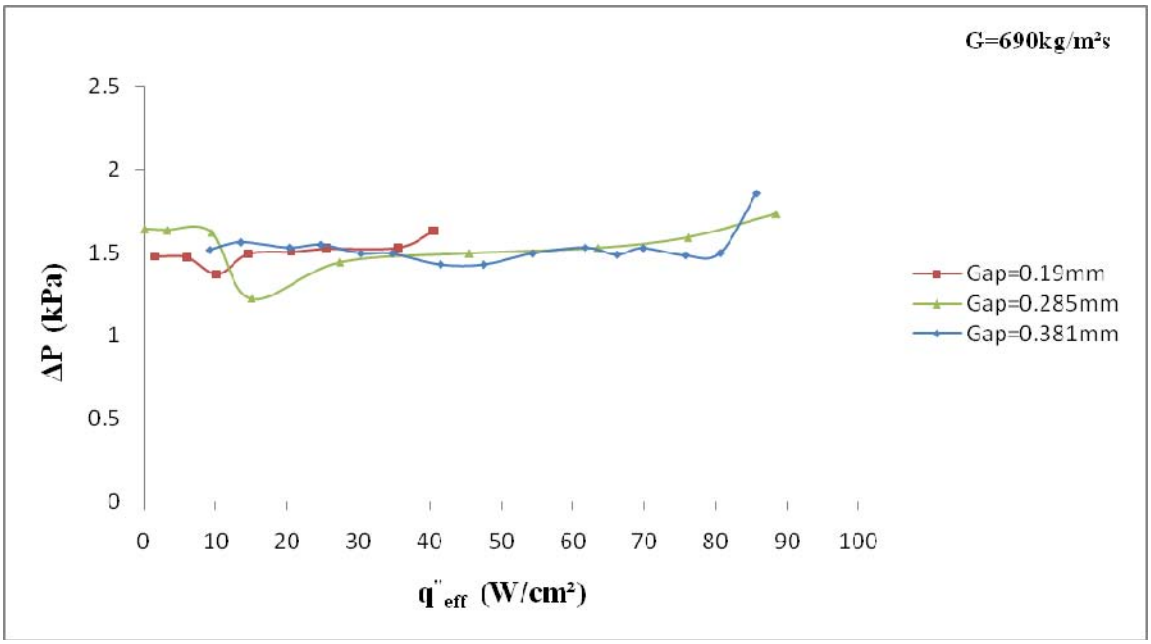

Figure 19: Effect of microgap dimensions on pressure drop at G=690kg/m²s.

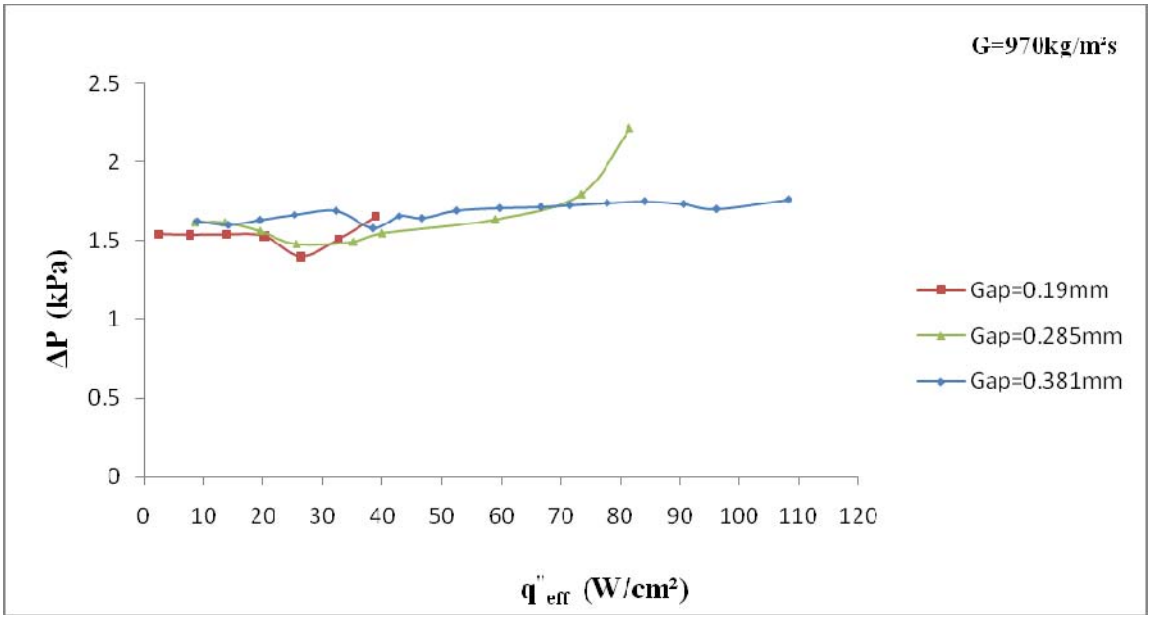

Figure 20: Effect of microgap dimensions on pressure drop at G=970kg/m²s.

4.1.2 Effect of Flow Rate

4.1.2.1 Boiling Curve

The effect of mass flux on boiling curve for micro gap size 0.19mm is shown in Figure 21. Tests were conducted on 190µm test section for three different mass fluxes ranging from 420 to 970 kg/m²s. At the onset of nucleate boiling the wall temperature exhibits a sudden change in slope from its single-phase. At low heat fluxes, the slopes of all boiling curves are fairly constant, indicative of single-phase heat transfer while in the two-phase region, a modest rise of wall temperature can be seen for the further increment of heat flux. At higher mass flux, boiling data give deteriorated performance with the increase of heat flux.

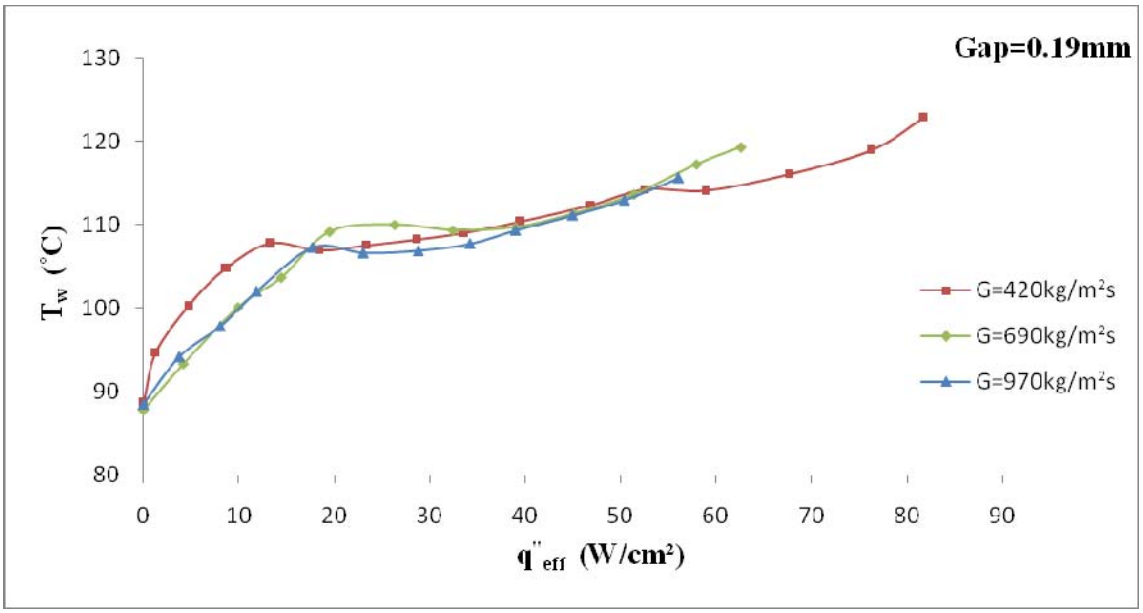

Figure 21: Boiling Curve for Gap dimension 0.19mm.

The effect of flow rate on boiling curve for micro gap size 0.285mm and 0.381mm are shown in Figure 22 and Figure 23. The onset of boiling can be identified in the figure as the point where the wall temperature exhibits a sudden change in slope from its single-phase dependence. The onset of boiling strongly depends on the mass flux, with a higher heat flux observed at ONB with increasing mass flux. The boiling data were independent of mass flux, indicating the nucleate boiling dominance.

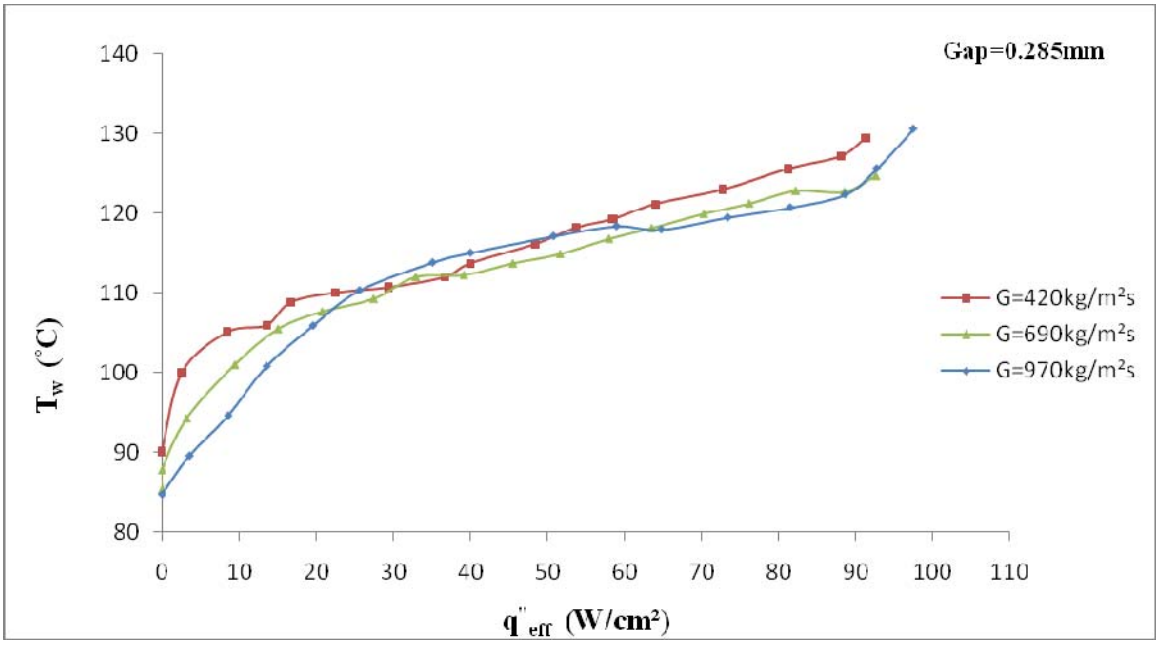

Figure 22: Boiling Curve for Gap dimension 0.285mm.

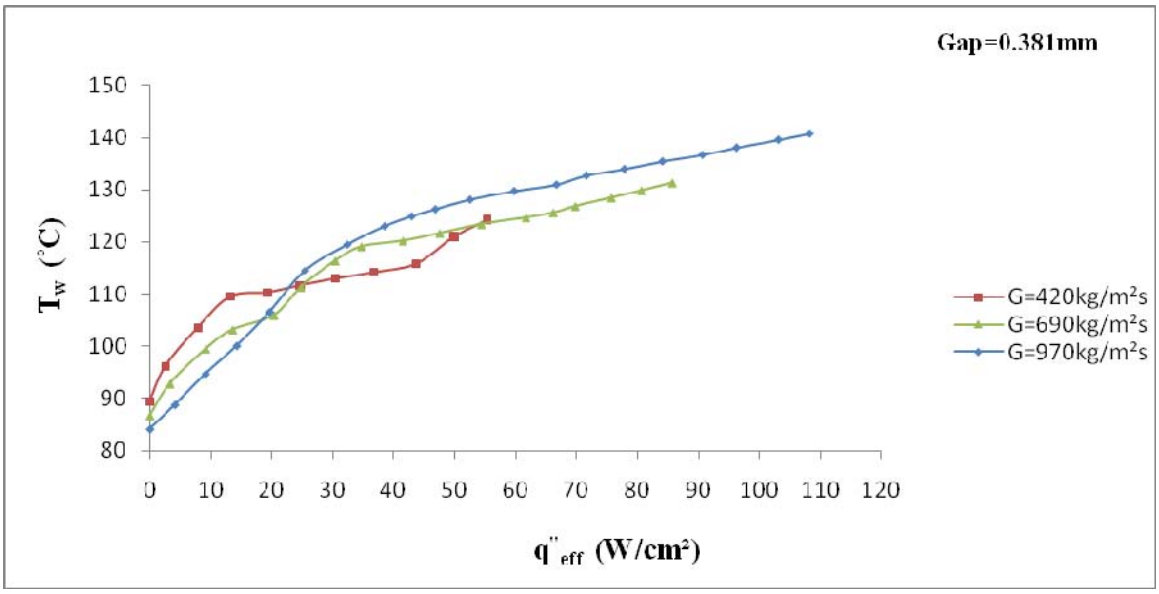

Figure 23: Boiling Curve for Gap dimension 0.381mm.

4.1.2.2 Local Heat Transfer Coefficient

The effect of mass flux on local heat transfer coefficient for microgap size 0.19mm is shown in Figure 24. The local heat transfer coefficient is calculated at position 15, the central diode in the last downstream location as indicated in Figure 8(c). The presence of local temperature sensors allows the local heat transfer coefficients to be computed. For low heat fluxes, the local heat coefficient increases almost linearly with heat flux. At higher heat fluxes, the curve shows a change in slope after the ONB as the heat transfer coefficient increase rapidly after boiling commences. It can be seen from figure that mass flux has a great influence on local heat transfer coefficient and the lowest mass flux leads to the highest value of heat transfer coefficient. This can be explained in the view of fact that at a given heat flux; the vapour quality at the outlet is higher for a lower mass flux. Thus, the local heat transfer coefficient increase significantly at lower mass flux.

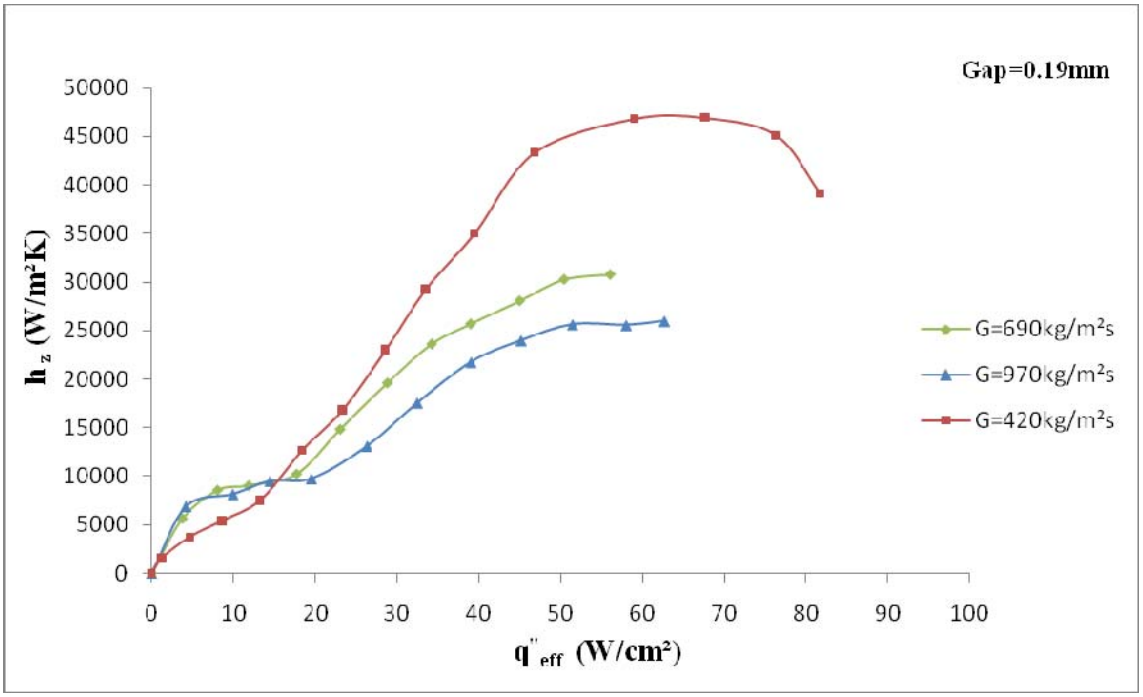

Figure 24: Effect of mass flux on local heat transfer coefficient for Gap dimension 0.19mm.

The effect of mass flux on local heat transfer coefficient for microgap size 0.285mm is shown in Figure 25. For low heat fluxes, the local heat coefficient increases almost linearly with heat flux. At higher heat fluxes, the curve shows a change in slope after the ONB as the heat transfer coefficient increase rapidly after boiling commences. It can be seen from figure that mass flux has a very little influence on local heat transfer coefficient. This may indicate the nucleate boiling is the dominance boiling mechanism for larger micro gap systems.

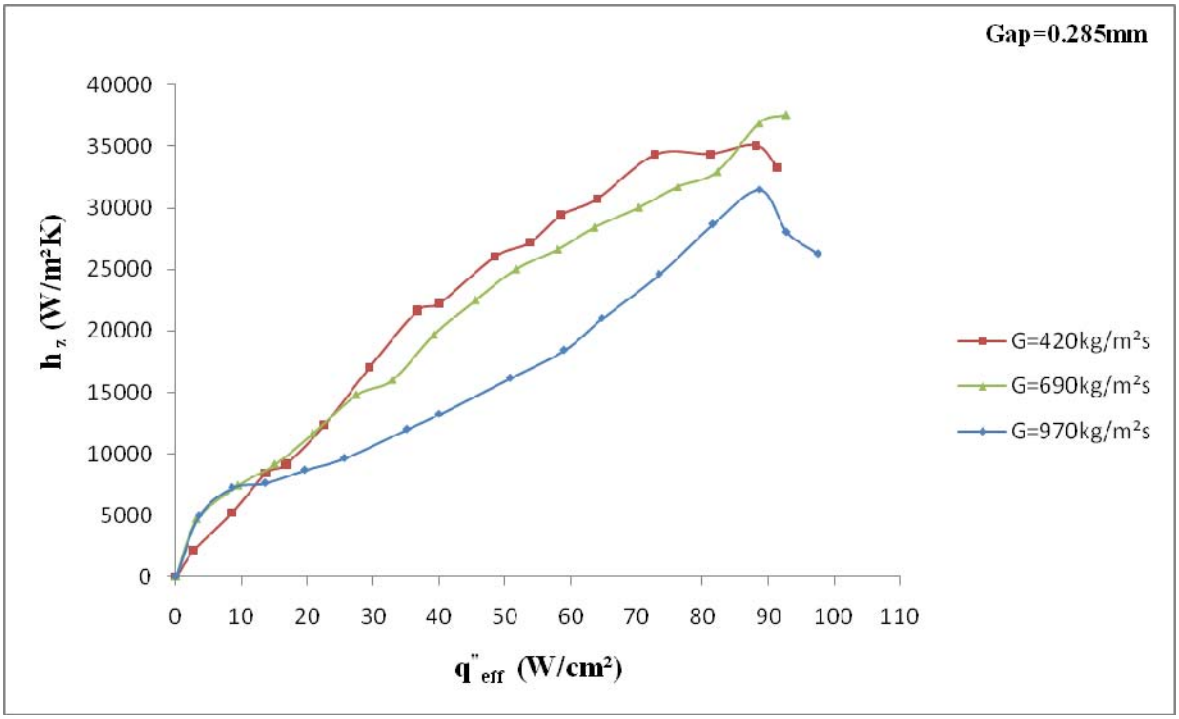

Figure 25: Effect of mass flux on local heat transfer coefficient for Gap dimension 0.285mm.

4.1.2.3 Pressure Drop

Figure 26 shows the variation of pressure drop with increasing heat flux for a range of mass fluxes for microgap size 0.19mm. It is observed from figure that for two-phase flow, for a fixed heat flux, pressure drop increase with increase of mass flux. The pressure drop increases with increasing vapour content but for the same heat flux, as the mass flux increases, the vapour content decreases, leading to the trends shown in Figure 26. For higher microgap size like 0.285mm and 0.381, as can be seen in Figures 27 and 28, higher pressure drop differences occur between different mass fluxes.

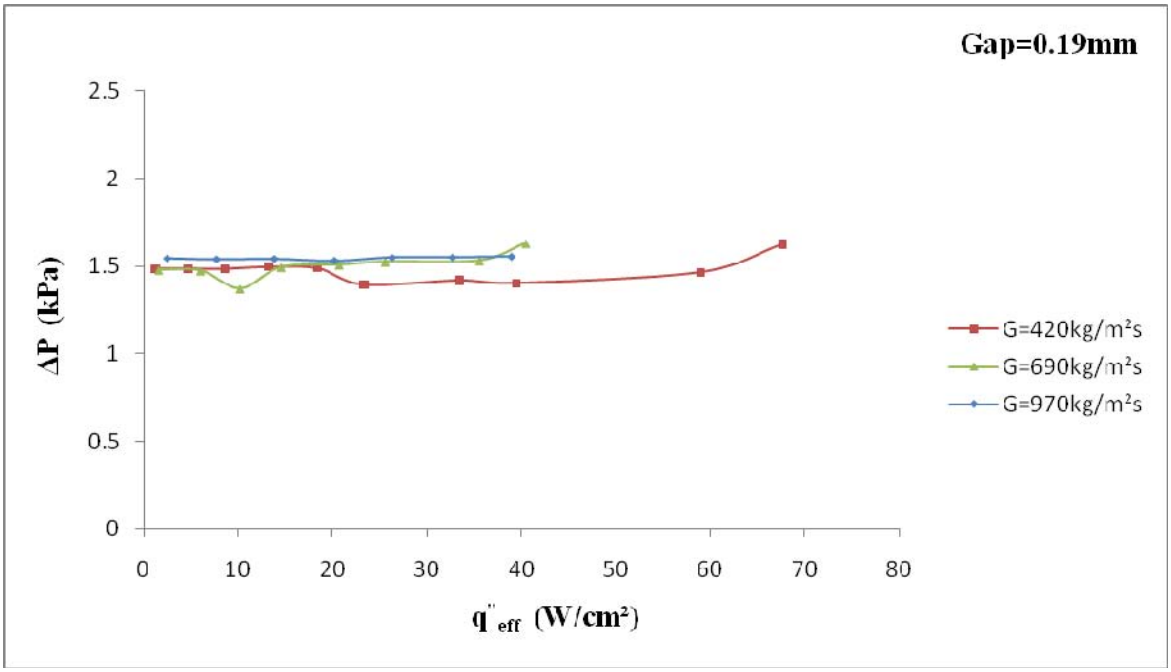

Figure 26: Effect of mass flux on Pressure Drop for Gap dimension 0.19mm.

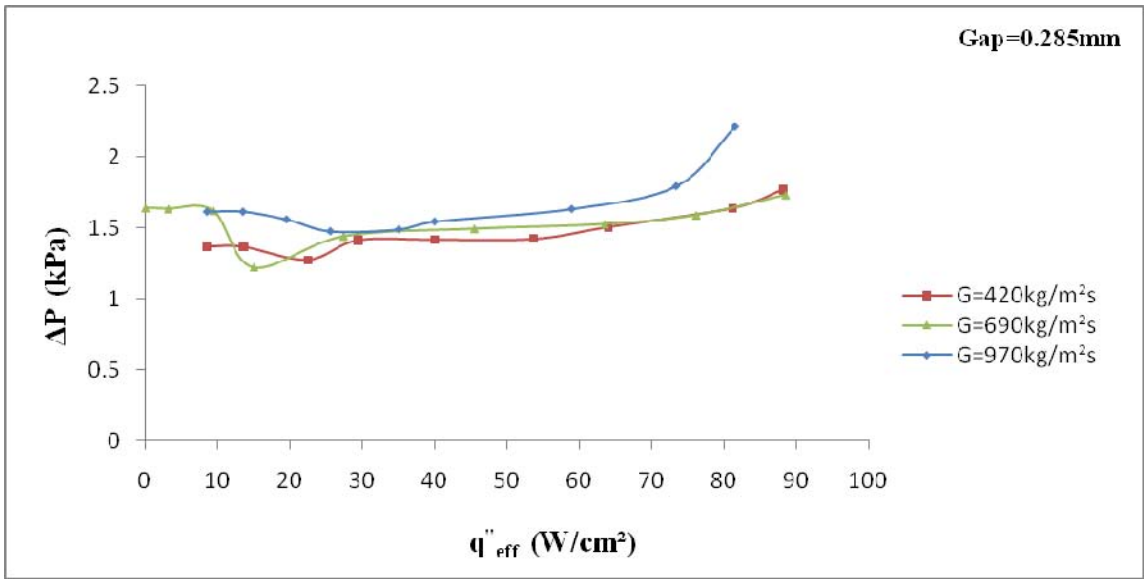

Figure 27: Effect of mass flux on Pressure Drop for Gap dimension 0.285mm.

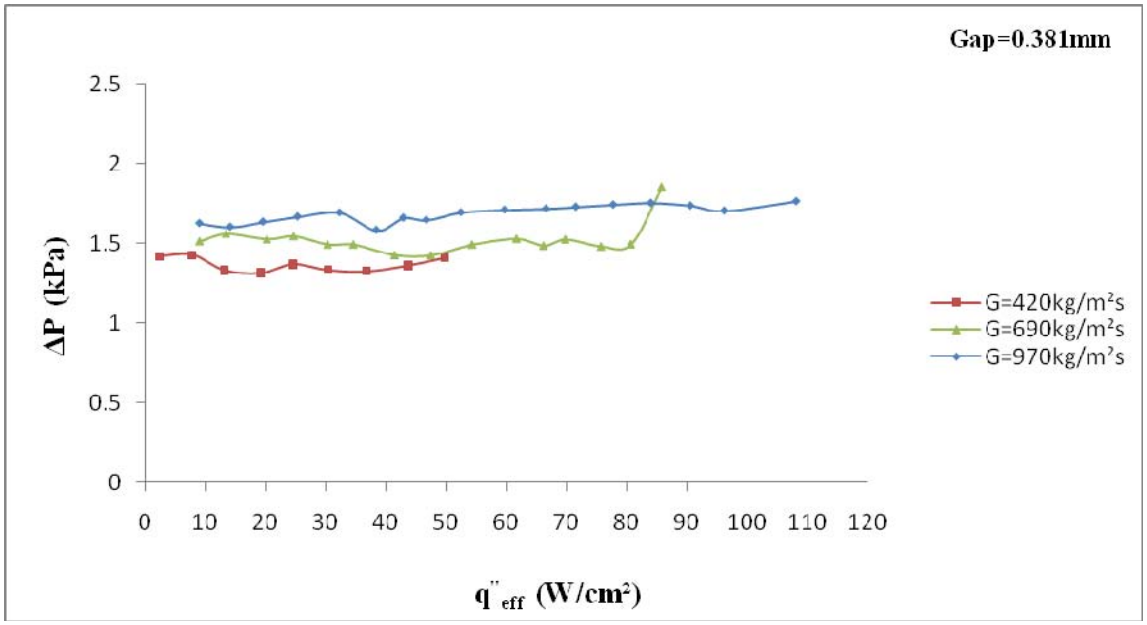

Figure 28: Effect of mass flux on Pressure Drop for Gap dimension 0.381mm.

4.2 Two-phase Microgap Channel Cooling Technology for Hotspots Mitigation

The boiling curve is plotted for water mass flux G=420 kg/m²s with test section of 190μm gap in terms of the variation of effective heat flux with the local wall temperature in Figure 29. At Figure 29, wall temperatures were taken at five streamwise locations along the center row with the diode sensors 11, 12, 13, 14 and 15 (locations shown in Fig. 8(c)). The onset of nucleate boiling (ONB) can be identified in the figures as the point where the wall temperature exhibits a sudden change in slope from its single-phase dependence. At low heat fluxes, the slopes of all boiling curves are fairly constant, indicative of single-phase heat transfer. In the two-phase region, a modest rise in wall temperature can be seen for further increase of heat flux. In addition, the temperature across the chip is more uniform in the two-phase region as can be seen from the converging of the boiling curves. Similar trend has been observed by Lee et al [41]. From Figure, it can be seen that after ONB the wall temperature has a strong dependency on the heat flux for these microgap size. It indicates that convective boiling rather than nucleate boiling, are the main heat transfer mechanisms. In convective boiling, a thin liquid layers flowing along the outer walls of the channel and the vapour flows in the center of the channel called vapor core. Thin liquid layers have low resistance to thermal diffusion and evaporation of liquid into the vapor core can promote the removal of substantial thermal energy from the walls. As the layer thins, the heat transfer rate increases and reduce temperatures near hotspots.

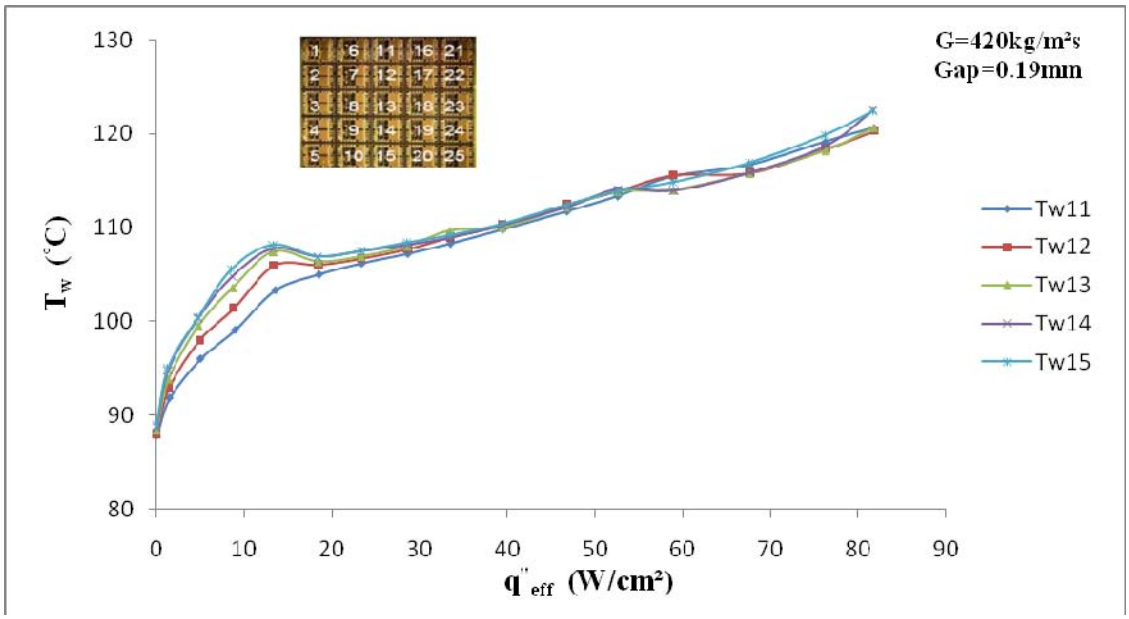

Figure 29: Flow Boiling Curve (streamwise locations along the centre row).

The boiling curve is plotted for water mass flux G=420 kg/m²s with test section of 381µm gap in terms of the variation of effective heat flux with the local wall temperature in Figure 30. At Figure 30, wall temperatures were taken at five spanwise locations with the diode sensors 5, 10, 15, 20 and 25 (locations shown in Fig. 8(c)). Trend matches with Figure 29. Before ONB, due to hot spot, some temperature nonuniformity was observed but after ONB, temperature was almost uniform.

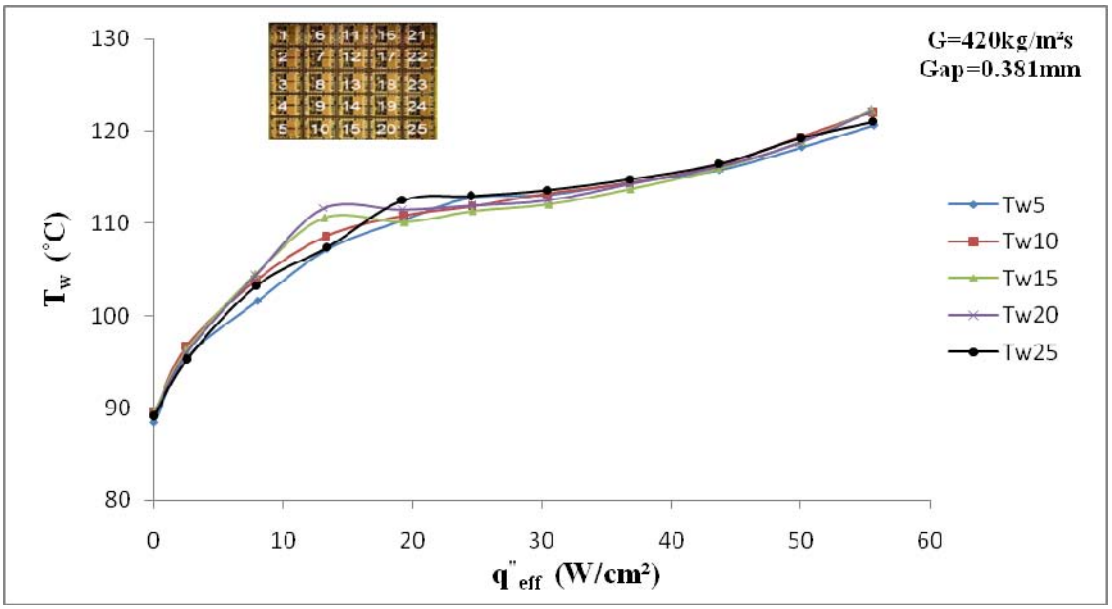

Figure 30: Flow Boiling Curve (spanwise locations).

The boiling curve is plotted for water mass flux G=420 kg/m²s with test section of 190µm gap in terms of the variation of effective heat flux with the local wall temperature in Figure 31. At Figure 31, wall temperatures were taken at five arbitrary locations on the silicon chip with the diode sensors 3, 10, 11, 19 and 24 (locations shown in Fig. 8(c)). Trend matches with Figure 29. Due to hot spot, temperature nonuniformity was observed at the beginning but after ONB, temperature was uniform through surface shown in fig 31. Thus two-phase flow boiling in microgap channel can be used for hot spot mitigation.

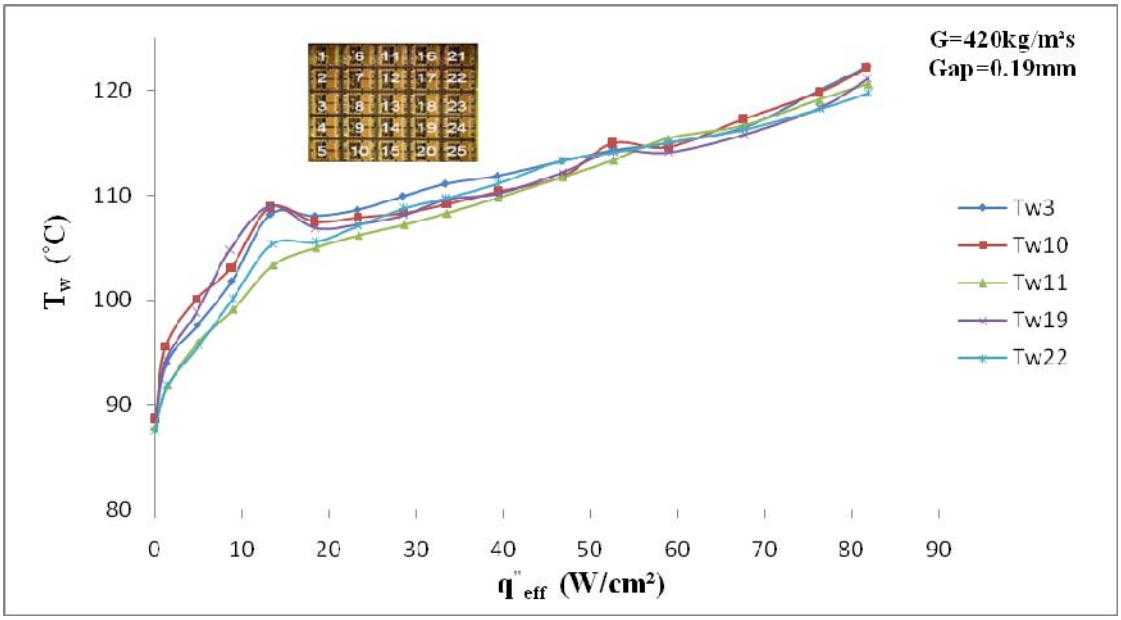

Figure 31: Flow Boiling Curve to show mitigating hotspots (arbitrary locations).

Comparison of wall temperature at single phase flow and two phase flow in 285µm gap for heat flux of 63.5W/cm² and mass flux of 690Kg/m²s is shown in Figure 32. In this figure, wall temperatures were taken at five spanwise locations with the diode sensors 5, 10, 15, 20 and 25 (locations shown in Fig. 8(c)). From figure, it can be seen clearly that two phase flow maintain a uniform wall temperature rather than single phase flow for same heat and mass flux. This is because; utilizing the latent heat of coolant, two phase flow boiling can dissipate significantly higher heat fluxes than its single phase counterpart.

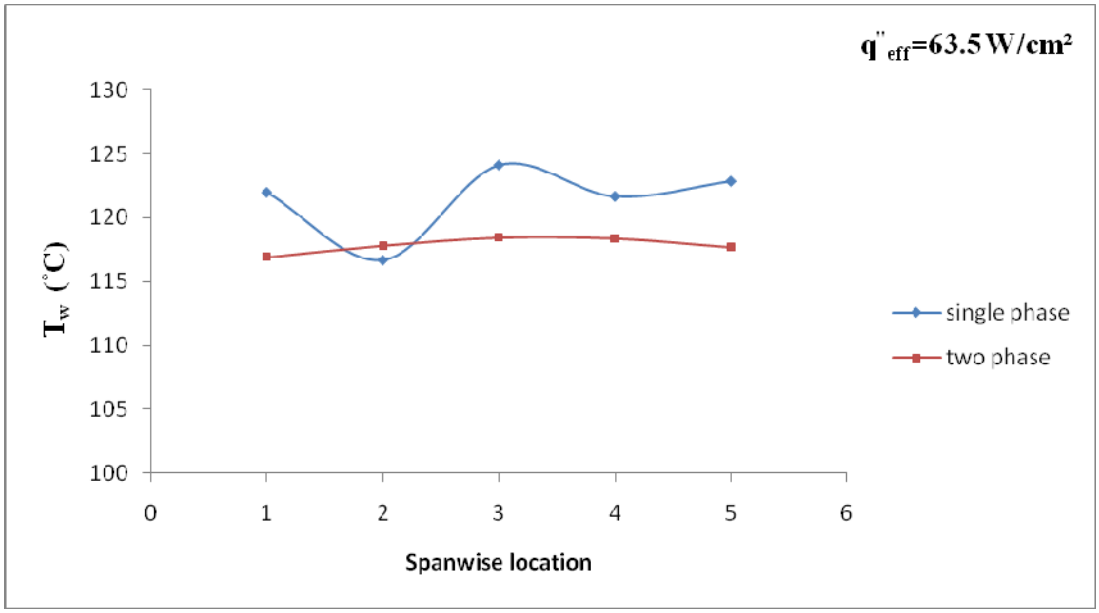

Figure 32: Comparison of wall temperature at single phase and two phase flow in Microgap.

Figure 33 shows the test chip wall temperature variation for different gap dimension at heat flux 57W/cm² and mass flux 420Kg/m²s. It can be seen from figure that smaller the gap dimension, more uniform the wall temperature. Moreover, smaller gap maintain lower wall temperature. Due to the smaller microgap size relative to the bubble diameter at departure, bubbles occupy the microgap creates confinement effects. So, instead of nucleate boiling, evaporation of thin liquid layer removes more heat from wall and maintains lower wall temperature for smaller gap.

Temperature variations on chip wall in microchannel and microgap channel are shown in Figure 34. Microgap cooler maintains uniform wall temperature rather than microchannel coolers at same heat and mass flux. According to Jae-MO Koo et al. [29] pressure drop is the most critical factor in design of microchannel heat sink and optimization should be performed to minimize pressure drop along the microchannels to reduce temperature variations. In this experiment, in microgap cooler, pressure drop is very negligible and maintain a uniform pressure field through the surface but in microchannel, large pressure drop occurs may the reason for large variation of temperature.

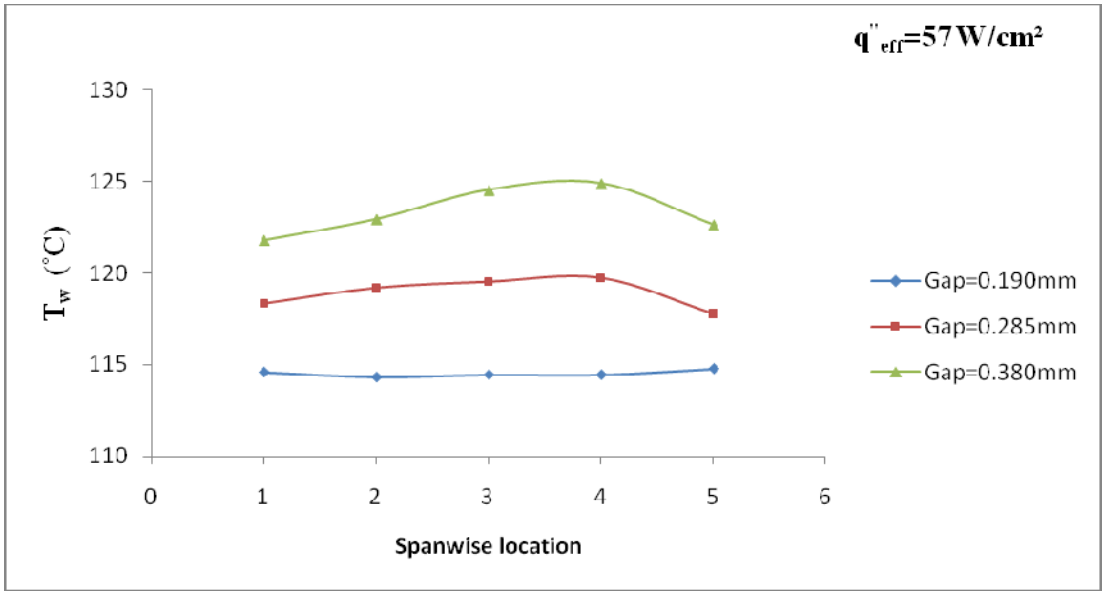

Figure 33: Comparison of wall temperature for different gap dimension.

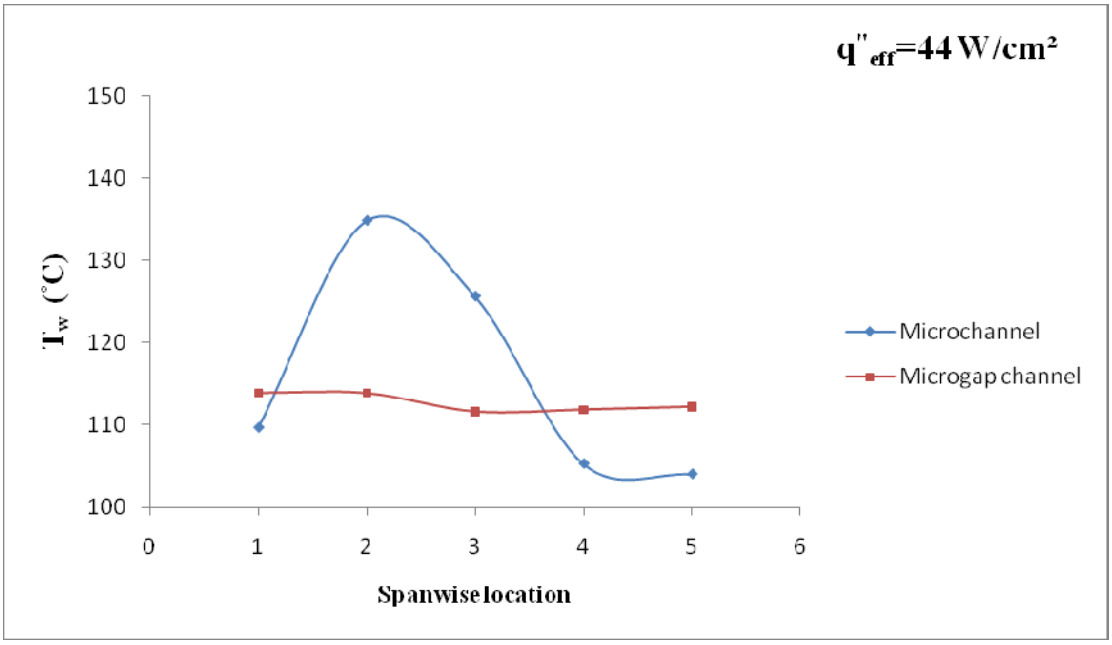

Figure 34: Comparison of wall temperature between Microchannel and Microgap channel.

4.3 Two-phase Microgap Coolers in Mitigating Flow Instabilities and Flow Reversal

Comparison of Inlet Pressure Instability in microchannel and Microgap channel at mass flux 420kg/m²s and heat flux 40W/cm² is plotted in Figure 35. Microchannel shows around 40% more inlet pressure instability than microgap channel. In a small size channel the vapor growth phase is limited in the radial direction because of the hydraulic diameter. Only the axial direction allows vapor growth when boiling occurs. On the other hand, in microgap, the vapour generated has room to expand both spanwise and downstream instead of being forced upstream which minimize the inlet pressure instability. Similar trend also has been observed for higher flow rate in Figures 36 and 37.

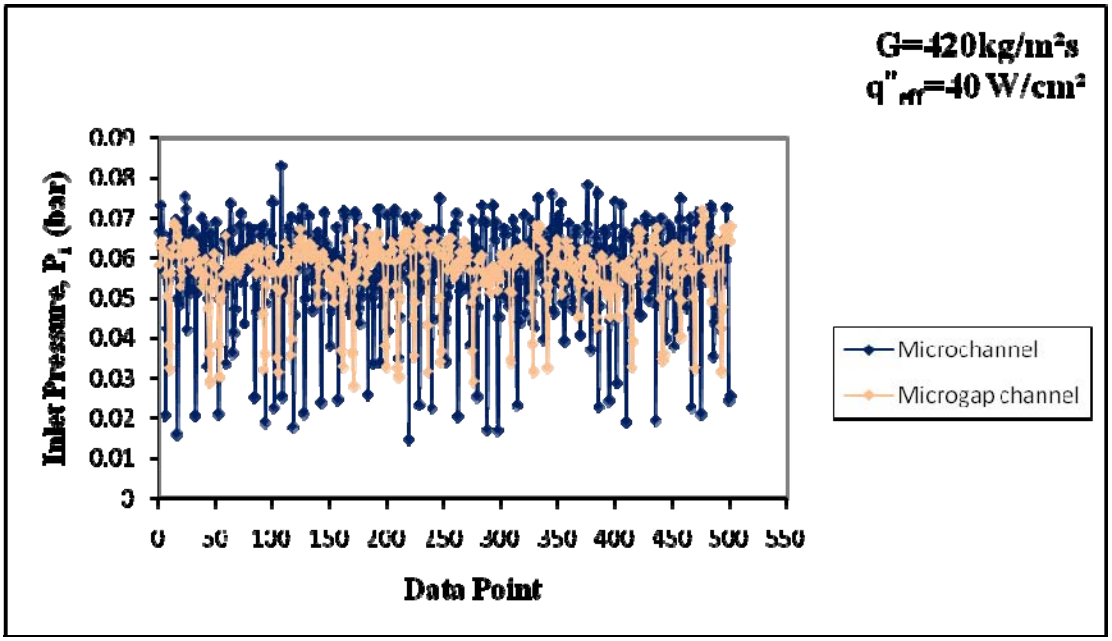

Figure 35: Comparison of Inlet Pressure Instability in micochannel and Microgap channel at mass flux 420kg/m²s.

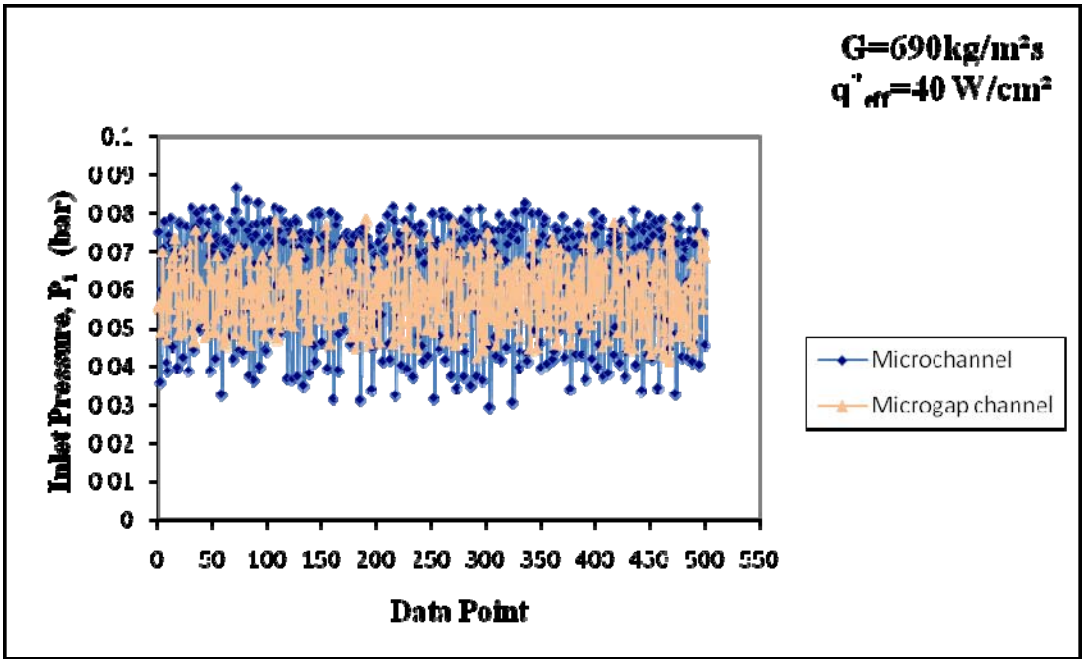

Figure 36: Comparison of Inlet Pressure Instability in micochannel and Microgap channel at mass flux 690kg/m²s.

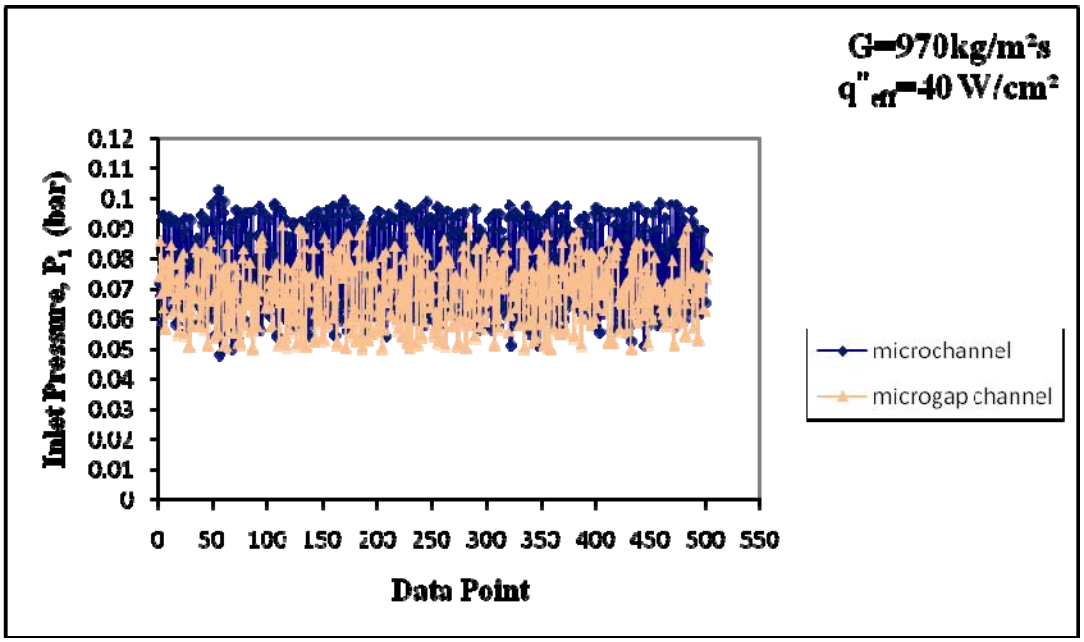

Figure 37: Comparison of Inlet Pressure Instability in micochannel and Microgap channel at mass flux 970kg/m²s.

4.4 Heat Transfer Characteristics in Microchannel

4.4.1 Boiling Curve

Boiling curves are plotted at three different mass fluxes for the test section with the microchannels of width 200µm as shown in Figure 38. From figure, it is observed in the single phase region that the lower the mass flux, the higher the wall temperatures for a given heat flux. Moreover, onset of nucleate boiling occurs at lower heat flux for a lower mass flux. After the onset of nucleate boiling, the boiling curves become insensitive to heat flux and mass flux. This observation may support the dominance of nucleate boiling in the microchannels. Similar phenomenon has been observed in Bertsch et al. [13] and Harirchian et al. [15]. At higher heat fluxes, the boiling curve again become sensitive to mass flux and wall temperature rise sharply with small increment of heat flux. This may be due to transition to slug flow and annular flow regimes at higher heat flux.

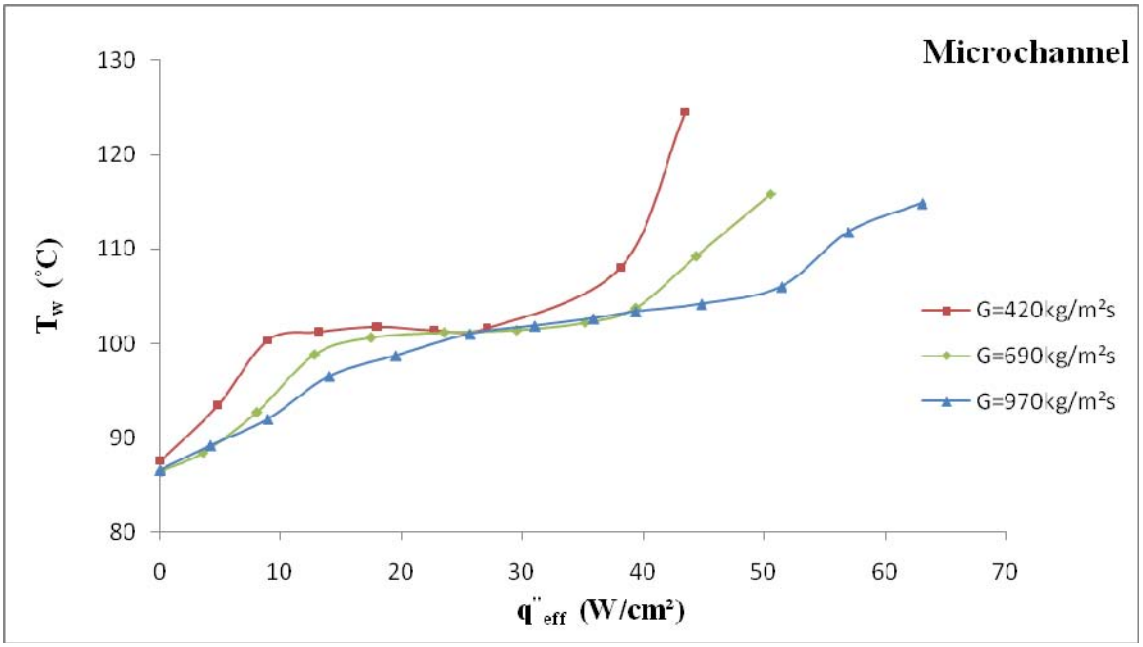

Figure 38: Boiling Curve for microchannels of width 200µm.

4.4.2 Local Heat Transfer Coefficient

The effect of mass flux on local heat transfer coefficient as a function of heat flux is shown in Figure 39. It can be seen from figure that at the single phase region, the heat transfer coefficient increase with mass flux for a fixed heat flux. The heat transfer coefficient becomes independent of mass flux after onset of nucleate boiling. At higher heat flux, the heat transfer coefficient again becomes dependent of mass flux as convective boiling begins to dominate that of nucleate boiling. The heat transfer coefficient starts to decrease with further increase of heat flux. This may be due to partial dryout that happen in microchannel wall with higher heat flux. Similar phenomenon has been observed by Harirchian et al. [15].

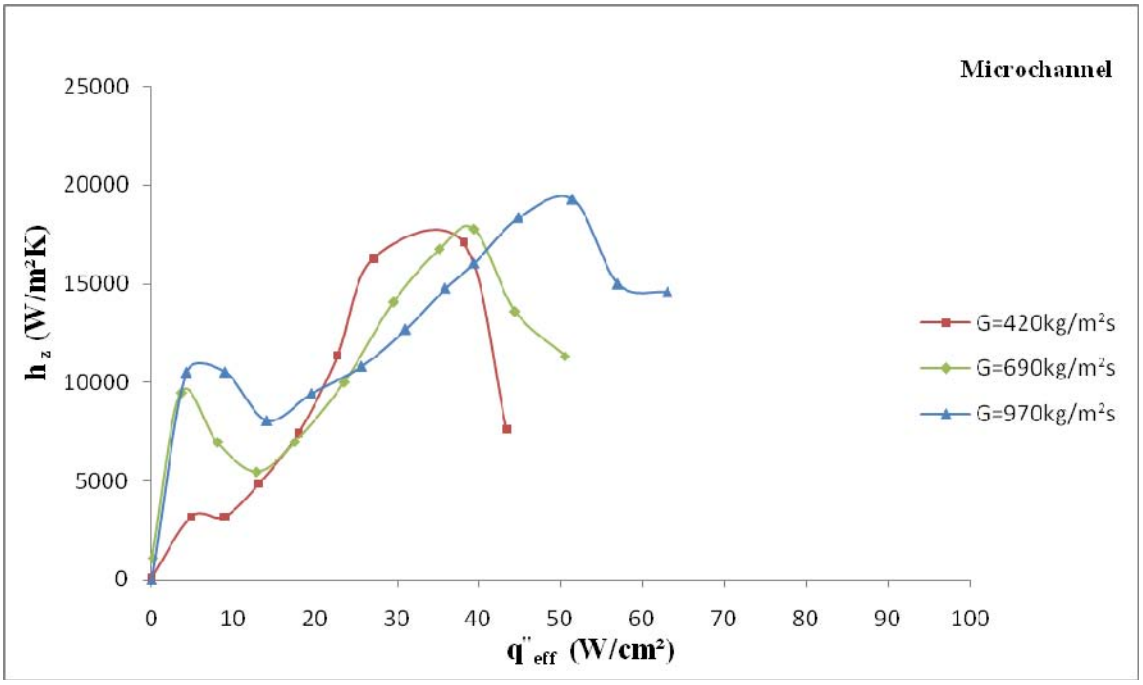

Figure 39: Effect of mass flux on local heat transfer coefficient for microchannels of width 200µm.

4.4.3 Pressure Drop

The effect of mass flux on pressure drop as a function of heat flux is shown in Figure 40. Tests were conducted on 200µm test section for three different mass fluxes ranging from 420 to 970 kg/m²s. From figure, it can be seen that in the single phase region, the pressure drop slightly decrease with increase of heat flux for all mass flux. This may be due to the reduction of liquid viscosity with the increase of liquid temperature. After the single phase region, pressure drop curves change the slope and increase with heat flux in two phase region. This may be due to the acceleration effect of vapor as well as the two phase frictional pressure drop. The pressure drop increase with increase of mass flux in both single and two phase regions. Similar phenomenon has been observed in Lee et al. [41] and Harirchian et al. [15].

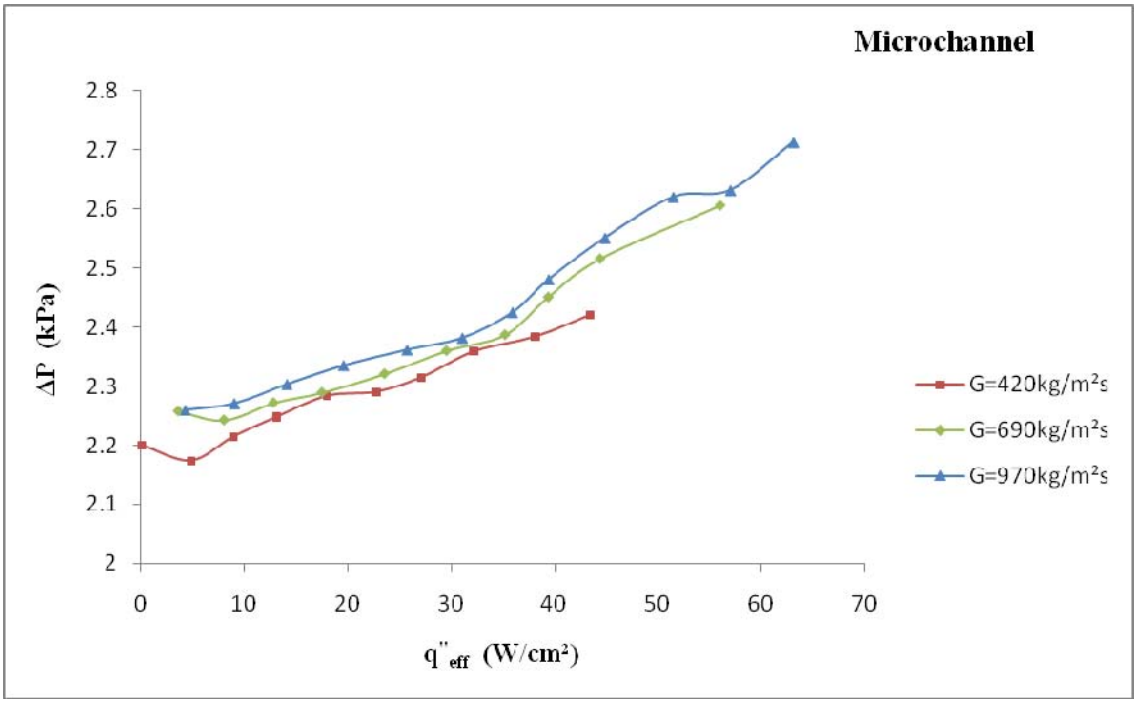

Figure 40: Effect of mass flux on pressure drop for microchannels of width 200µm.

4.5 Comparison of Heat Transfer Characteristics between Two-phase Microgap Coolers and Microchannel Coolers

4.5.1 Boiling Curve

Comparison of boiling curve between microchannel of width 200µm and microgap channel of gap 200µm is illustrated in Figure 41. Tests were conducted for same mass flux and inlet fluid temperature. As can be seen from figure, for the same heat flux microchannel coolers gives the lower surface temperature than the microgap coolers. In microchannel test section, fluid gets more surface area to flow and can remove more heat from surface may be the reason for lower surface temperature. After the onset of nucleate boiling in microchannel, boiling curve become insensitive of heat flux may support the dominance of nucleate boiling. On the other hand, after the onset of nucleate boiling in microgap channel, the boiling curve shows sensitivity on heat flux and wall temperature increase gradually with heat flux may support the dominance of convective boiling. In microchannel, at higher heat fluxes, the boiling curve again become sensitive to heat flux and wall temperature rise sharply with small increment of heat flux. This may be due to partial dryout at higher heat flux in microchannel.

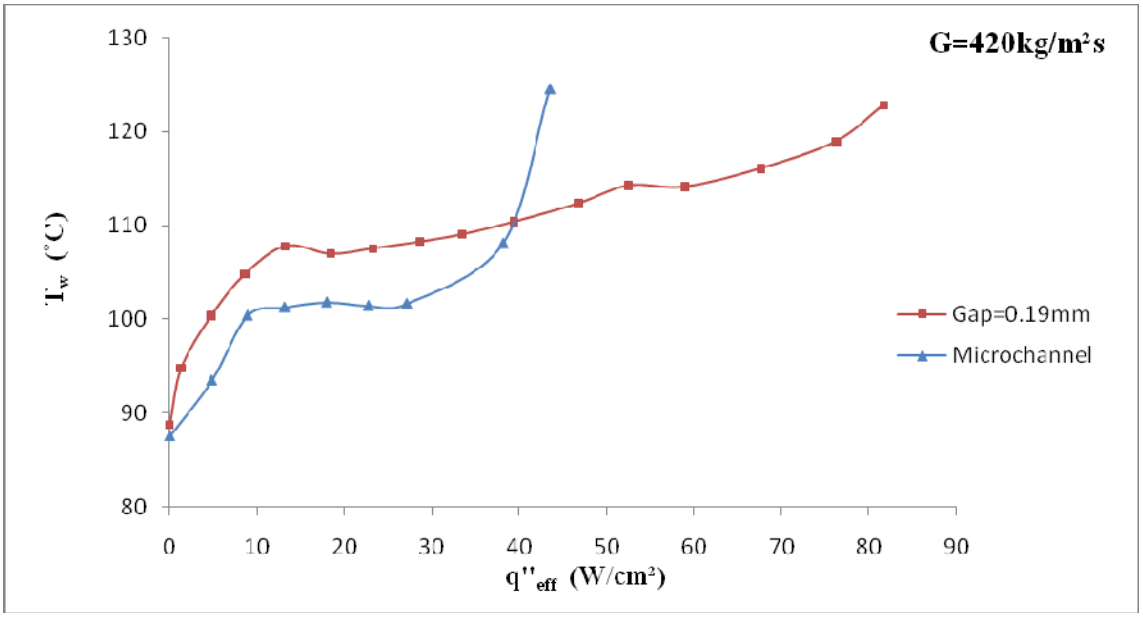

Figure 41: Comparison of boiling curve between Microchannel and Microgap channel.

Similar phenomenon has been observed in Figures 42 and 43 for higher mass flux of 690 kg/m²s and 970 kg/m²s respectively.

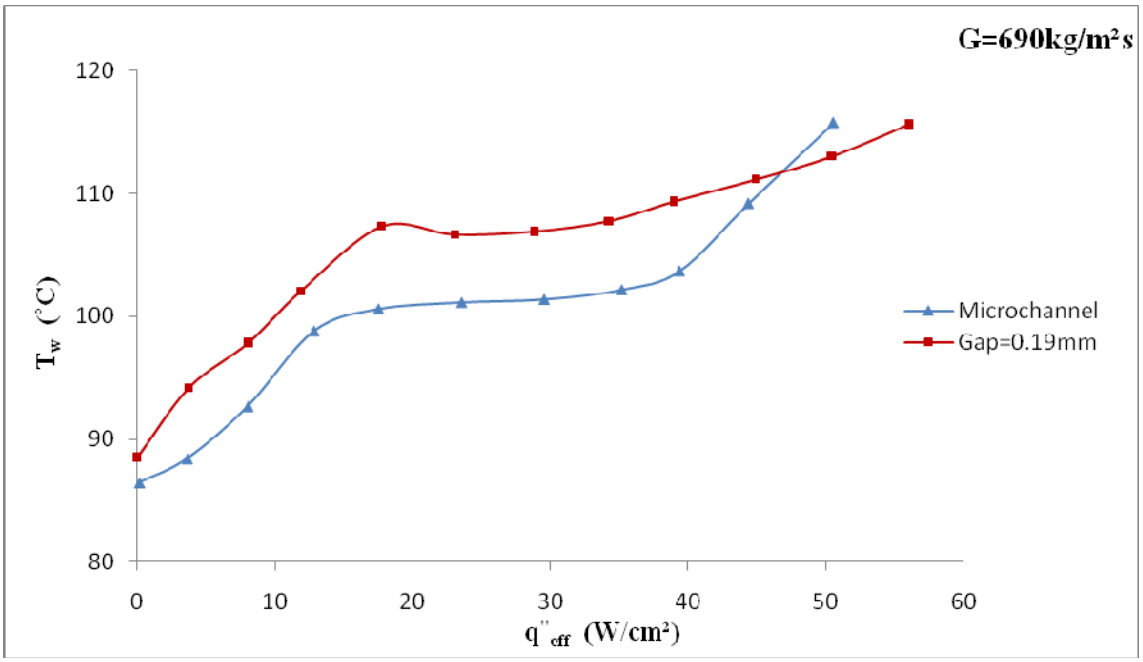

Figure 42: Comparison of boiling curve between Microchannel and Microgap channel.

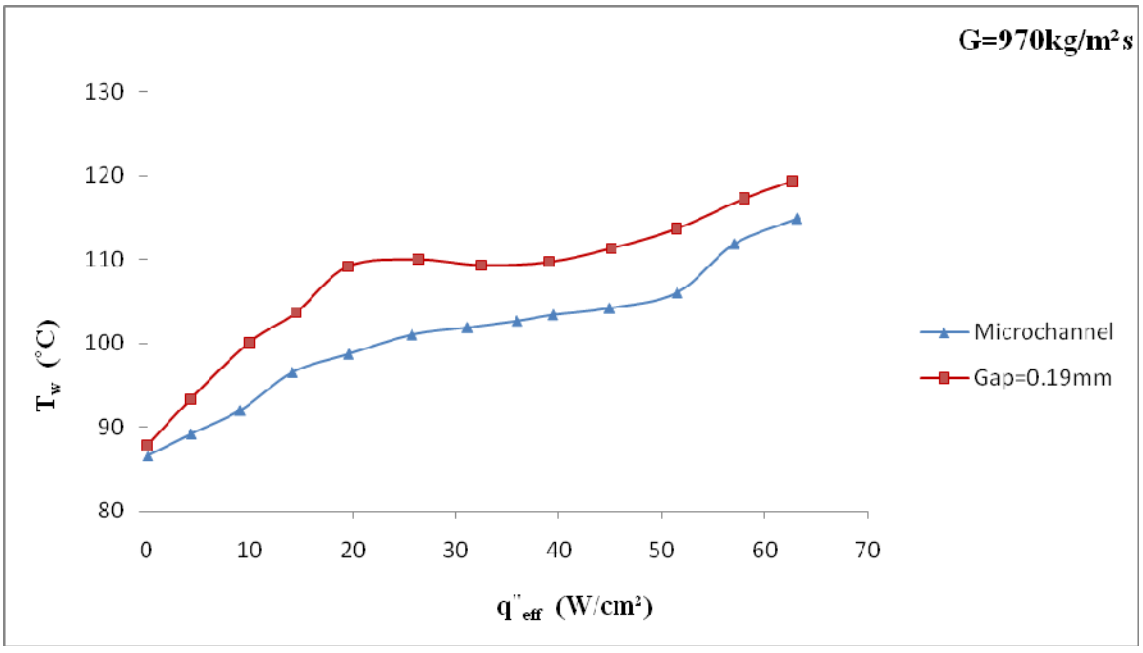

Figure 43: Comparison of boiling curve between Microchannel and Microgap channel.

4.5.2 Local Heat Transfer Coefficient

Comparison of local heat transfer coefficient between microchannel of width 200µm and microgap channel of gap 200µm is presented in Figure 44. Tests were conducted for mass flux 420 kg/m²s. It can be seen from figure that the heat transfer coefficient increase with increasing heat flux. In single phase region, heat transfer coefficient is almost identical for microchannel and microgap channel for mass flux 420 kg/m²s. But in two phase region, heat transfer coefficient is higher in microgap channel rather than microchannel cooler. In microchannel, nucleate boiling is the dominant boiling mechanism. In microgap, bubble nucleation at the walls is not the only heat transfer mechanism, and the evaporation of this liquid film at the walls in the slug and annular flows also contributes to the heat transfer. Therefore, the value of local heat transfer coefficient is larger for this microgap.

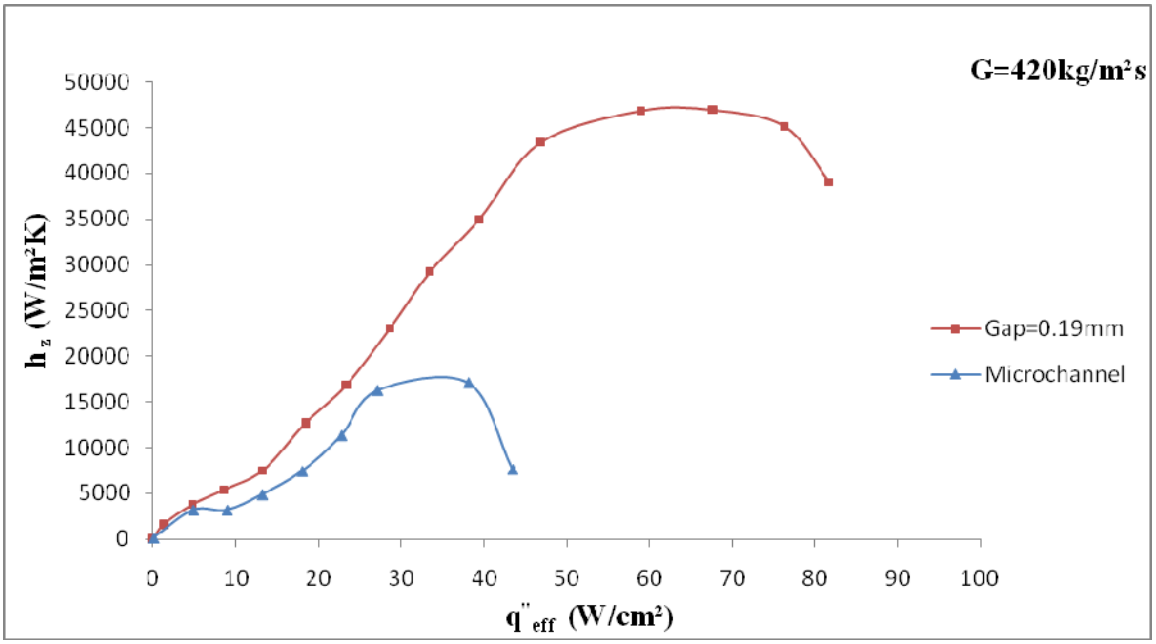

Figure 44: Comparison of local heat transfer coefficient between Microchannel and Microgap channel.

Similar phenomenon has been observed in Figures 45 and 46 for higher mass flux of 690 kg/m²s and 970 kg/m²s respectively. In the single phase region, microchannel gives higher heat transfer coefficient as fluid gets more surface area to flow and can remove more heat from surface but in two phase region, microgap gives better performance because of convective boiling nature. Moreover, with the increase of mass flux, the differences in the performance of two test section become smaller. This is because, in microgap channel, the

vapour quality at the outlet is lower for a higher mass flux for a fixed heat flux which may minimize the confinement effect at higher mass flux.

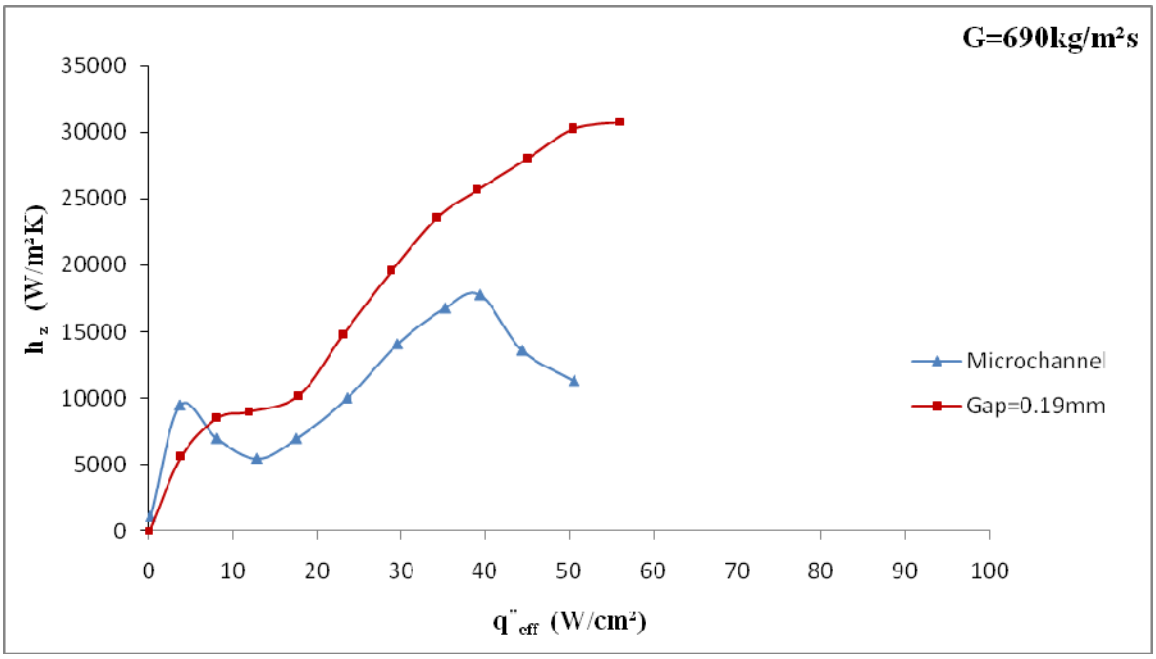

Figure 45: Comparison of local heat transfer coefficient between Microchannel and Microgap channel.

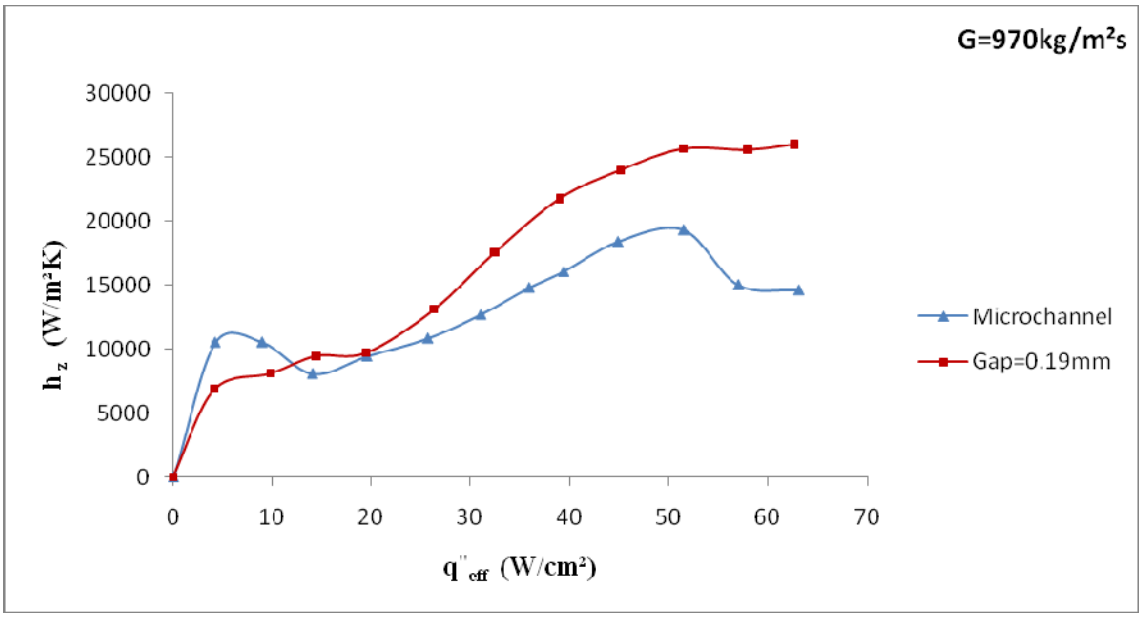

Figure 46: Comparison of local heat transfer coefficient between Microchannel and Microgap channel.

4.5.3 Pressure Drop

Comparison of pressure drop between microchannel of width 200µm and microgap channel of gap 200µm as a function of heat flux is presented in Figure 47. Tests were conducted for mass flux 420 kg/m²s. Pressure drop is higher for microchannel test section than microgap test section in both single phase and two phase regions. In two phase region, slope of the pressure drop line of microchannel is also higher than microgap channel for same heat flux.

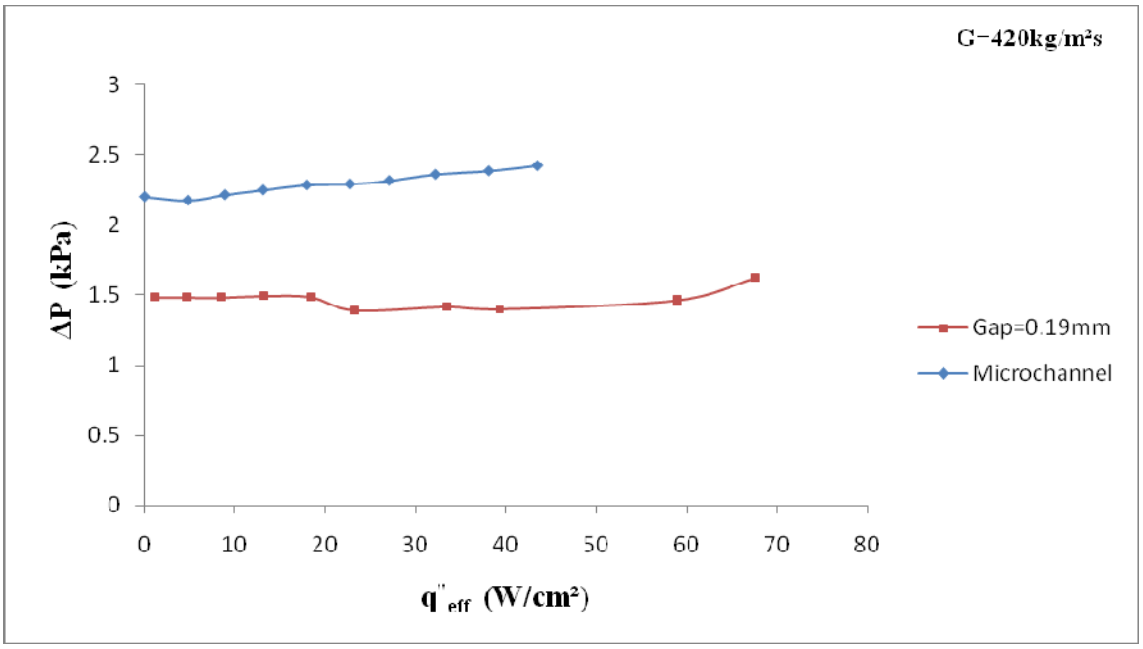

Figure 47: Comparison of pressure drop between Microchannel and Microgap channel.

Similar phenomenon has been observed in Figures 48 and 49 for higher mass flux of 690 kg/m²s and 970 kg/m²s respectively.

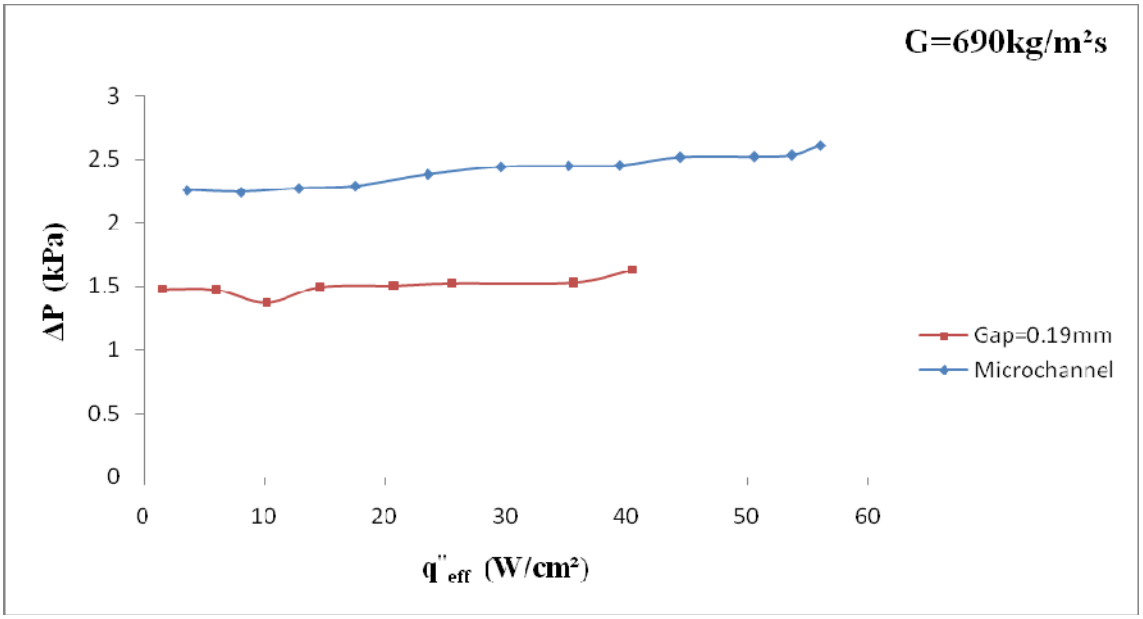

Figure 48: Comparison of pressure drop between Microchannel and Microgap channel.

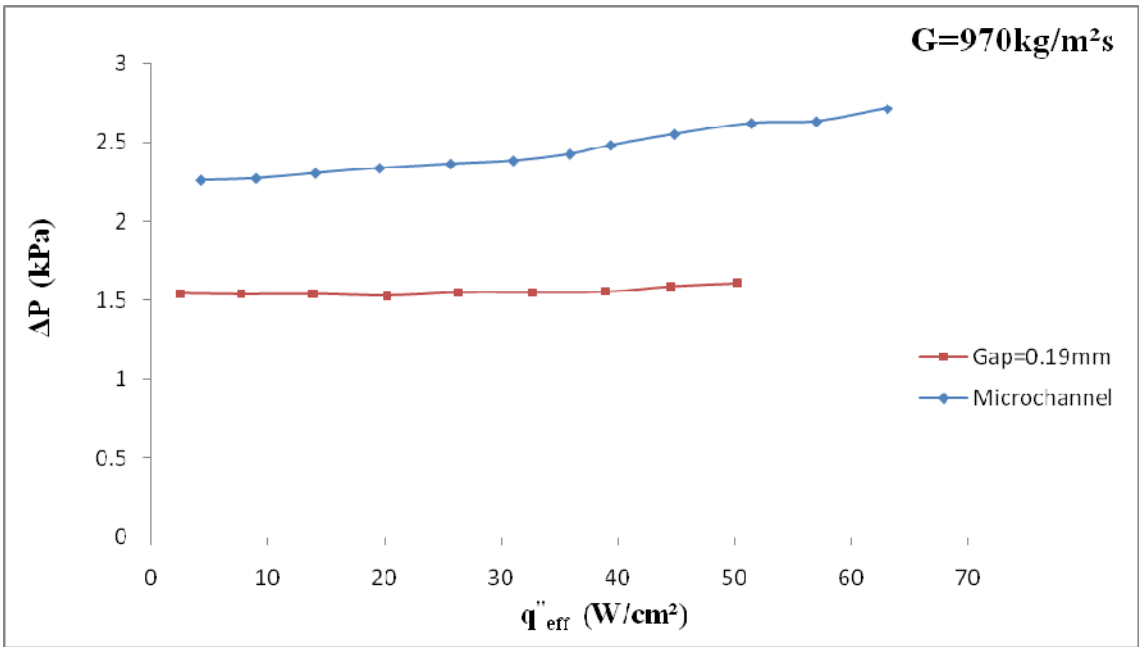

Figure 49: Comparison of pressure drop between Microchannel and Microgap channel.

4.6 Conclusions

In this study, experiments have been performed in order to examine two-phase flow boiling in a silicon microgap based heat sink having gap height of 190μm, 285μm and 380μm, using water with inlet temperature of 86˚C. The effects of mass flux and heat flux on heat transfer coefficient and pressure drop characteristics were examined by varying mass flux ranging from 420 Kg/m²s to 970 Kg/m²s and effective heat flux up to 100 W/cm². An array of integrated micro-temperature sensors allows local heat transfer coefficients to be determined. The fluid temperatures and pressure drop across the microgap array were also measured. The size effects on different parameters have been investigated. The extensive microgap boiling experiments and analysis has led to some important findings:

- At low heat fluxes, the slopes of all boiling curves are fairly constant, indicative of single-phase heat transfer while in the two-phase region, a modest rise of wall temperature can be seen for the further increment of heat flux.
- After the onset of nucleate boiling, the wall temperatures show a week dependency on heat flux. As further increase of heat flux, the wall temperatures become dependent of heat flux and the boiling curves deviate for different gap size.
- This strong dependence of the wall temperature on the heat flux for these microgap sizes for low mass flux indicate that convective boiling rather than nucleate boiling, are the main heat transfer mechanisms.
- For higher mass flux, the smaller microgap size shows more dependency of wall temperature on heat flux rather than higher gap size.
- In small microgap size, bubble nucleation at the walls is not the only heat transfer mechanism, and the evaporation of this liquid film at the walls in the slug and annular flows also contributes to the heat transfer. Therefore, the value of local heat transfer coefficient is larger for this smaller gap.
- With the decrease of microgap size, the heat transfer coefficient increased until it reached a maximum, after which it deteriorated with decreasing gap size as CHF values and boiling data show deteriorated performance [39].
- In the single phase region, pressure drop decreases slightly with increasing heat flux as the fluid viscosity decreases with the increase of fluid temperature. In the two phase region, the pressure drop increases with increasing heat flux as vapour content increase with the increase in temperature of the fluid.

- The pressure drop increases with decreasing the microgap size. But for all mass fluxes and gap sizes, pressure drops are very low comparative to other micro channels.
- The effect of mass flux can be seen for 190μm microgap. The onset of boiling strongly depends on the mass flux, with a higher heat flux observed at ONB with increasing mass flux. Moreover, at higher mass flux, boiling data gives deteriorated performance. Mass flux has a great influence on local heat transfer coefficient also and the lowest mass flux leads to the highest value of heat transfer coefficient.
- For higher gap, the boiling data and local heat transfer coefficient are independent of mass flux, indicating the nucleate boiling dominance.
- For two-phase flow subjected to a fixed heat flux, pressure drop increases with the increase of mass flux.
- Due to hot spot, temperature nonuniformity was observed at the beginning but after ONB, temperature was uniform through surface. Thus, two-phase flow boiling in microgap channel can be used for hot spot mitigation.
- Microchannel shows around 40% more inlet pressure instability than microgap channel.
- In the single phase region, microchannel gives higher heat transfer coefficient as fluid gets more surface area to flow and can remove more heat from surface but in two phase region, microgap gives better performance because of convective boiling nature.
- Pressure drop is higher for microchannel test section than microgap test section in both single phase and two phase regions.

5. Future Work Plan

The proposed research focuses on the fundamental study of flow boiling and heat transfer in microgap channel through careful and systematic experimental investigations over a range of channel dimensions, heat fluxes, mass fluxes and vapor qualities. The temperature and pressure data obtained will allow a better understanding of the flow boiling mechanism in the micro-scale domain.

Flow visualization using a high speed camera will be conducted to closely examine the flow boiling in different microgap channel. This high speed flow visualization will led to a detailed mapping of flow regimes and the dynamic nature of two-phase flow within microgap channel.

Flow regime maps are commonly used to determine the flow patterns that exist under different operating conditions, as well as the conditions for flow pattern transitions. Such maps are essential to the development of flow regime-based models for the prediction of the heat transfer rate and pressure drop in flow boiling. Despite the inability of macroscale boiling maps or adiabatic two-phase flow regime maps to predict the boiling flow patterns in microchannels or microgap, a review of the literature shows a dearth of investigations into flow regime maps specifically targeted at microchannels or microgap undergoing flow boiling that are applicable to a wide range of microgap dimensions and experimental conditions. The effects for a wide range of experimental parameters e.g. microgap dimensions, mass flux, fluid properties on flow boiling regimes and heat transfer rates will be investigated further.

Experimental investigation will be first carried out with de-ionized water as the coolant. Further investigations will be conducted later with other coolants as well to study the effects of thermophysical properties on the flow boiling performance. This would contribute to a generalized understanding of two-phase flow and heat transfer behaviours in micro/mini-channels.

Experimental measurement for saturated flow boiling in microgap channel will be compared with various recent existing correlations from literature to verify their respective accuracies.

Nomenclature

A	footprint area, cm²
A_c	total wetted area of the microchannels, cm²
c_p	specific heat, J/kg ˚C
d	depth of microchannel, µm
G	mass flux, kg/m²s
h	heat transfer coefficient, W/m²K
H	gap height, µm
h_{fg}	heat of vaporization, J/kg
k_s	thermal conductivity, W/cm°C
L	length of the substrate, cm
$\dot{m}$	mass flow rate, kg/s
N	number of microchannels
P	pressure, bar
ΔP	pressure drop, bar
Q	flow rate, ml/min
q	total heat dissipation, W
q_{eff}	effective heat dissipation, W
$q_{1}{}_{eff}{}^{1}$	effective heat flux, W/cm²
q_{loss}	heat loss, W
T	temperature, °C
t	substrate thickness, cm
V_d	voltage drop across diode, V
W	width of the substrate, cm
w	channel width, µm
x	thermodynamic quality
x	x-coordinate, cm
x_e	local thermodynamic equilibrium quality
x_{exit}	exit quality
y	y-coordinate, cm

z	z-coordinate (axial distance), cm

Greek

η	fin Efficiency

Subscripts

avg	average
d	diode
f	liquid
g	vapor
h	heater
i	manifold inlet
o	manifold outlet
s	substrate
sat	saturated
sp	single-phase
t	thermal
tp	two-phase
w	wall
z	local

References

[1] J. Lee, I. Mudawar, Low-temperature two-phase microchannel cooling for high-heat-flux, Thermal Management of Defense Electronics, IEEE Transactions on Components and Packaging Technologies, Article in press.

[2] H. Pokharna, K. Masahiro, E. DiStefanio, R. Mongia, B. J. Crowley, W. Chen, M. Izenson, Microchannel cooling in computing platforms: performance needs and challenges in implementation, Second International Conference on Microchannels and Minichannels, ICMM (2004) 109-118.

[3]S.G. Kandlikar, A. V.Bapat, Evaluation of jet impingement, spray and microchannel chip cooling options for high heat flux removal, Heat Transfer Engineering 28(11) (2007) 911–923.

[4] K.A. Triplett, S.M. Ghiaasiaan, S.I. Abdel-Khalik, A. Lemouel, and B.N. McCord, Gas-liquid two-phase flow in microchannels part II: void fraction and pressure drop, International Journal of Multiphase Flow 25 (1999) 395-410.

[5] A. Bar-Cohen and E. Rahim, Modeling and prediction of two-phase refrigerant flow regimes and heat transfer characteristics in microgap channel, Heat Transfer Engineering 30 (8) (2009) 601 – 625.

[6] G. Hetsroni, Handbook of Multiphase Systems, Hemisphere Publishing Co. (1982).

[7] S. S. Mehendal, A. M. Jacobi and R. K. Shah, Fluid flow and heat transfer at micro- and meso-scales with application to heat exchanger design, Applied Mechanics Review 53 (2000) 175-193.

[8] S. G. Kandlikar, Two-phase flow patterns, pressure drop and heat transfer during boiling in minichannel and micro-channel flow passages of compact heat exchangers. In: Compact Heat Exchangers and Enhancement Technology for the Process Industries, Begell House New York (2001) 319-334.

[9] P. A. Kew, and K. Cornwell, Correlations for Prediction of Boiling Heat Transfer in Small-Diameter Channels, Applied Thermal Engineering 17 (1997) 705-715.

[10] Tannaz Harirchian, Suresh V. Garimella, A comprehensive flow regime map for microchannel flow boiling with quantitative transition criteria, International Journal of Heat and Mass Transfer, Article in press.

[11] S.V. Garimella, C.B. Sobhan, Transport in microchannels – a critical review, Annual Review of Heat Transfer 13 (2003) 1–50.

[12] J.R. Thome, Boiling in microchannels: a review of experiment and theory. International Journal of Heat Fluid Flow 25 (2004) 128–139.

[13] S.S. Bertsch, E.A Groll, S.V. Garimella, Review and comparative analysis of studies on saturated flow boiling in small channels, Nanoscale and Microscale Thermophysical Engineering 12 (2008) 187–227.

[14] Sehwan In, Sangkwon Jeong, Flow boiling heat transfer characteristics of R123 and R134a in a micro-channel, International Journal of Multiphase Flow 35 (2009) 987–1000.

[15] T. Harirchian, S.V. Garimella, Microchannel size effects on local flow boiling heat transfer to a dielectric fluid, Int. J. Heat Mass Transfer 51 (2008) 3724–3735.

[16] T. Chen, S.V. Garimella, Measurements and high-speed visualizations of flow boiling of a dielectric fluid in a silicon microchannel heat sink, International Journal of Multiphase Flow 32 (2006) 957–971.

[17] A. E. Bergles, Review of instabilities in two-phase Systems. In: Proc, NATO Advanced Study Institute, Istanbul, (1) (1976) 383–422.

[18] M. Ishii, Study on flow instabilities in two-phase flow mixtures, Report ANL 76–23, Argonne National Laboratory (1976).

[19] G. Yadigaroglu, Two-phase flow instabilities and propagation phenomena. In: Delhaye J.M., Goit M., Riethmuller M.L. (Eds.), Thermohydraulics of Two-phase Systems for Industrial Design and Nuclear Engineering (1981).

[20] L. Tadrist, Review on two-phase flow instabilities in narrow spaces, International Journal of Heat and Fluid Flow 28 (2007) 54–62.

[21] S.G. Kandlikar, M.E. Steinke, S. Tian, and L.A. Campbell, High speed photographic observation of flow boiling of water in parallel mini-channels, paper presented at the ASME National Heat Transfer Conference, Los Angeles, CA, (2001) 10-12.

[22] S.G. Kandlikar and P. Balasubramanian, An experimental study on the effect of gravitational orientation on flow boiling of water in 1054 x197 μm parallel mini-channels, Journal of Heat Transfer, ASME 127 (2005) 820–829.

[23] G. Hetsroni, D. Klein, A. Mosyak, Z. Segal, and E. Pogrebnyak, Convective Boiling in Parallel Micro-channels, First International Conference on Micro-channels and Mini-channels, Rochester, NY, ICMM (2003) 59–67.

[24] Y. Peles, Two-phase flow in micro-channels – instability issues and flow regime mapping, First International Conference on Micro-channels and Mini-channels, Rochester, NY, ICMM (2003) 559–566.

[25] C.-J. Kuo, Y. Peles, Pressure effects on flow boiling instabilities in parallel microchannels, International Journal of Heat and Mass Transfer 52 (2009) 271–280.

[26] S.G. Kandlikar, W.K. Kuan, D.A. Willistein, J. Borrelli, Stabilization of flow boiling in micro-channels using pressure drop elements and fabricated nucleation sites, Journal of Heat Transfer, ASME 128 (2006) 389-396.

[27] C.T. Lu and C. Pan, Stabilization of flow boiling in microchannel heat sinks with a diverging cross-section design, Journal of Micromechanics and Microengineering 18 (2008).

[28] W. Qu, Two-phase cross-connected micro-channel heat sink, United States Patent US 2009/ 0139701, 2009.

[29] J. Koo, L. Jiang, A. Bari, L. Zhang, E. Wang, T. W. Kenny, J. G. Santiago, K. E. Goodson, Convective boiling in microchannel heat sinks with spatially-varying heat generation, Thermal and Thermomechanical Phenomena in Electronic Systems (2002), ITherm (2002) 341-346.

[30] E.S. Cho, J.-M. Koa, L. Jiang, R. S. Prasher, M. S. Kim, J. G. Santiago, T. W. Kenny, and K. E. Goodson, Experimental study on two-phase heat transfer in microchannel heat sinks with hotspots, Semiconductor Thermal Measurement and Management Symposium, 2003, 242–246.

[31] A. Bar-Cohen and E. Rahim, Modeling and prediction of two-phase refrigerant flow regimes and heat transfer characteristics in microgap channels, Proceedings of the 5th International Conference on Nanochannels, Microchannels and Minichannels Rochester, NY, ICNMM (2007) 1141-1160.

[32] D.-W. Kim, E. Rahim, A. Bar-Cohen and B. Han, Thermofluid characteristics of two-phase flow in micro-gap channels, 11th IEEE Intersociety Conference on Thermal and Thermomechanical Phenomena in Electronic Systems, I-THERM (2008) 979-992.

[33] D.-W. Kim, E. Rahim, A. Bar-Cohen and B. Han, Direct submount cooling of high-power LEDs, IEEE Transactions on Components and Packaging Technologies, Article in Press.

[34] Jessica Sheehan, Avram Bar-Cohen, Spatial and temporal wall temperature fluctuations in two-phase flow in microgap coolers, Proceedings of the ASME 2010 International Mechanical Engineering Congress & Exposition, IMECE (2010) 12-18.

[35] http://www.delphi.com/manufacturers/auto/micro/flipchip/availability/pst102/

[36] R.D. Blevins, Applied Fluid Dynamics Handbook, Krieger Pub. Co. (1992) 77-78.

[37] D. Chislom, L.A. Sutherland, Prediction of pressure gradients in pipeline systems during two-phase flow, in: Symposium in Two-phase Flow Systems, University of Leeds, 1969.

[38] J.R. Taylor, An Introduction to Error Analysis, second ed., University Science Books, 1997.

[39] K.J.L. Geisler, A. Bar-Cohen, Confinement effects on nucleate boiling and critical heat flux in buoyancy-driven microchannels, International Journal of Heat and Mass Transfer 52 (2009) 2427–2436.

[40] K.A. Triplett, S.M. Ghiaasiaan, S.I. Abdel-Khalik, A. Lemouel and B.N. McCord, Gas-liquid two-phase flow in microchannels part I: two-phase flow patterns, International Journal of Multiphase Flow 25 (1999) 377-394.

[41] P.S. Lee and S.V. Garimella, Saturated flow boiling heat transfer and pressure drop in silicon microchannel arrays, International Journal of Heat and Mass Transfer 51 (2008) 789–806.